IONIZATION STRUCTURE AND EMISSION LINE INTENSITIES OF SEYFERT GALAXY NUCLEI

Thesis by

Gregory Alan Shields

In Partial Fulfillment of the Requirements

for the Degree of

Doctor of Philosophy

California Institute of Technology

Pasadena, California

1973

(Submitted October 16, 1972)

To

Captain Video

ACKNOWLEDGEMENTS

I am deeply indebted to my advisor, Professor J. B. Oke, for his constant encouragement and assistance. I thank J. N. Bahcall for suggesting this project and guiding its early phases, and G. Garmire, J. Gunn, G. Münch, W. Sargent, L. Searle, and D. Shaffer for valuable discussions. Many other people, both faculty and students, have helped to make my study at Caltech an inspiring and enjoyable experience. H. Holloway and S. Robinson kindly assisted with the typing. Finally, I am grateful to the National Science Foundation for support as a Graduate Fellow.

ABSTRACT

The ionizing radiation spectrum, geometry, and chemical abundances of the nuclei of the Seyfert galaxies NGC 1068 and 3C 120 are studied with the aid of detailed computer models. These objects represent opposite extremes of the Seyfert galaxy spectral types, but analysis indicates that they are similar in ionizing radiation and nebular geometry. The quantitative success of the models for the high excitation lines supports the idea that photoionization by a central continuum source is the ionization mechanism. However, the low excitation lines may indicate the importance of another process. The most attractive explanation of the observations of both 3C 120 and NGC 1068 involves ionizing radiation similar to that from a black body at 175,000° K with a radius of about 1 a.u, rather than an exponential or power law continuum. Most of the mass (10^5-10^6 $M_\odot$) is contained in a region of gaseous filaments with densities up to about 10^6 cm^{-3} and a radius near 50 pc, which constitutes the entire emission line region of NGC 1068 and the narrow line region of 3C 120. The broad permitted emission lines of 3C 120 come from an additional region of dense, narrow filaments with velocities up to 10^4 km s^{-1} located about a parsec from the continuum source. 3C 120 probably has the abnormally large helium abundance

N(He)/N(H) = 0.22, but observations are suggested to test an alternative hypothesis involving X-ray ionization. Important constraints provided by existing radio, infrared, and X-ray observations are discussed, and the importance of ultraviolet measurements is emphasized.

TABLE OF CONTENTS

TABLE OF CONTENTS

TABLE OF CONTENTS

I. INTRODUCTION

This thesis describes my attempts to understand the optical spectra of the Seyfert galaxies NGC 1068 and 3C 120.

Seyfert (1943) described a class of galaxies with broad emission lines coming from a central nucleus barely if at all resolved by the largest telescopes. To avoid definitions that are strongly dependent on the distance to an object, greater emphasis now is placed on spectroscopic rather than morphological characteristics. Hence, the term Seyfert galaxy presently includes objects with stellar or nearly stellar images, which are surrounded at least by some fuzziness presumed to be a galaxy, and which have spectra characterized by strong, broad emission lines and a strong UV continuum. The emission lines typically include recombination lines of H and He, and forbidden lines of N, O, Ne, and S. The relative intensities of these lines indicate a high degree of excitation. For example, (1) He II λ4686 is stronger than He I λ5876, (2) [O III] λ5007 is much stronger than [O II] λ3727, and [Ne V] λ3426 is at least comparable in strength to [Ne III] λ3869. A large range of ionization is often present, as may be shown by the presence of [O I] and [Ne V] emission from the same object.

The nuclei of Seyfert galaxies range in luminosity

from much fainter than to much brighter than the surrounding galaxy. Those in Seyfert's (1943) paper typically are several magnitudes fainter than the galaxies, but a continuous sequence of spectroscopically similar objects can be traced in increasing luminosity to the point where the surrounding galaxy is barely visible because of its faintness relative to the nucleus. It seems natural to speculate that the QSO's continue this sequence to even higher luminosities.

One of the striking features of Seyfert nuclei is the great breadth of the emission lines. Seyfert galaxies have been grouped into two classes according to the emission line profiles (Weedman 1972). In one class, the prototype for which is NGC 1068, the permitted and forbidden lines have similar profiles with half-widths of order 2000 km s^{-1}. In the case of NGC 1068, similar structure in both the permitted and forbidden line profiles suggests that these lines arise from the same moving clouds of gas. In the other type, exemplified by NGC 4151, the forbidden emission lines have widths of around 100-300 km s^{-1}, while the permitted lines have cores with similar widths surrounded by very broad wings extending to as much as 10^4 km s^{-1} from the line center. The essential point is that there is a wide range in the relative intensities of the broad and narrow components from invisibility of the narrow component of the permitted lines in extreme NGC 4151 type

objects to invisibility of the wings in the other extreme.

The absence of broad wings from the forbidden line profiles has been taken to mean that the wings of the permitted lines arise in a region where the electron density is so high that the forbidden line emission is collisionally suppressed relative to the permitted line emission. The breadth of the permitted line wings has been attributed to Doppler shifts resulting either from rapid mass motions of the emitting gas or from multiple scatterings by electrons. Facts confronting the electron scattering hypothesis include (1) large predicted Balmer line self-absorption that is not observed (Rees and Sargent 1972), and (2) a lower limit to the size of the permitted line region in 3C 120 (Shields, Oke, and Sargent 1972) that rules out electron scattering in that object. The combined evidence seems to favor the mass motion explanation.

A useful model of the gas in Seyfert nuclei is to think of two distinct components (Souffrin 1968): (1) a narrow line region (NLR) which radiates the forbidden lines and the narrow cores of the permitted lines, and which typically has a density of 10^3-10^6 cm^{-3}; and (2) a broad line region (BLR) which radiates the broad permitted line wings and has a density of more than 10^8 cm^{-3}. On this picture, 3C 120 has the permitted line flux from the BLR

much greater than that from the NLR, whereas in NGC 1068 the BLR radiates very weakly or is absent altogether. The key point in this model is the correlation between high velocity and high density.

Interest in Seyfert galaxies has grown recently because of the possibility that the QSO's are distant and luminous Seyfert galaxies. The resemblence between the spectroscopically deduced properties of Seyfert nuclei and QSO's is remarkable. In each case, an ionized nebula having dimensions of the order of 10-100 pc, gas densities ranging from less than 10^4 to 10^8 cm^{-3} or more, and velocities up to 10^4 km s^{-1}, is associated with a compact source of nonstellar continuum. The continuum intensity is comparable to that of the nebular emission, and it may change in times as short as months. Both Seyfert galaxies and QSO's may have strong or weak radio emission, and there is a striking similarity between some Seyfert galaxies and quasars with rapidly variable radio components with flat spectra. In addition, X-rays have been detected from Seyfert galaxies and quasars.

There are several indications that photoelectric absorption of an ultraviolet continuum is largely responsible for the ionization and heating of the gas in Seyfert nuclei (Souffrin 1969) and QSO's. The nonstellar continuum of these objects, extrapolated to ionizing frequencies,

generally would be sufficient to account for the ionization and thermal balance. This property is reflected in the rough correlation of continuum and emission line intensities over several orders of magnitude in luminosity (Searle and Sargent 1968). Also, the electron temperatures indicated by line ratios are typical of photoionized nebulae, and are much lower than those required to produce the observed degree of ionization by thermal electron collisions. Consequently, in this work I have considered only photoionized models.

A decade of intense study of Seyfert galaxies and quasars has failed to achieve a basic understanding of these objects or their relationship. Although these are among the most powerful phenomena known in the universe, their source of energy remains a mystery. We do not know how long they last, whether they occur in ordinary or only very special galaxies, or in the case of the QSO's whether they occur in galaxies at all.

The theoretical understanding of the Seyfert phenomenon may be approached in one of two ways. One approach is to consider the entire class of objects and to try to understand the range of observed appearances. Another approach is to consider individual cases in detail, and then to compare the results for different objects.

A computer program which calculates the spectrum of emission line intensities in an assumed model is a convenient tool to use in either approach. Such a program can yield the intensities of a large number of lines useful to test the details of a specific model; and it can calculate families of models to study the observable consequences of changes in the chemical abundances, density, motion, and location of the gas, and in the ionizing radiation spectrum.

One reason to study NGC 1068 and 3C 120 is that these two objects represent extremes in the observational properties of Seyfert galaxies. NGC 1068 has a low redshift ($z = 0.0036$) and a Seyfert nucleus much fainter than the surrounding, well studied galaxy. On the other hand, 3C 120 has a redshift ten times greater, and the nucleus far outshines the galaxy, about which little is known. NGC 1068 has a spectrum characterized by the absence of relative weakness of broad emission line wings, whereas the broad components strongly dominate the permitted lines of 3C 120. Thus these two objects represent opposite extremes of the division into the NGC 1068 type and the NGC 4151 type. Interest in NGC 1068 is further increased by the availability of high resolution photoelectric spectrum scans made possible by the high apparent brightness of the nucleus. Interest in 3C 120

is heightened by the resemblence of its radio source to some quasars, including an apparently relativistic expansion, and by the unusual strength of its helium emission lines.

This study differs from previous photoionization model calculations in a number of ways. The most detailed previous work has been applied to Crab nebula filaments (Williams 1967) and to QSO's (Bahcall and Kozlovsky 1971a, b; Davidson 1972; MacAlpine 1972). This study deals with Seyfert galaxies having substantially different spectral properties observed in a different wavelength interval. The studies of NGC 1068 and NGC 4151 by Williams and Weymann (1968) and of NGC 4151 by MacAlpine (1971) discussed only a few models but were important because they showed that the photoionization mechanism was promising and should be considered in greater detail. Improvements in the present work include the following: (1) a full consideration of black body and exponential ionizing continua, whereas the investigations cited above used almost exclusively power law continua; (2) a systematic exploration of possible nebular geometries and densities assisted by the use of simplifying homology relations; (3) the use of more accurate observational data and of reddening corrections which substantially alter important line ratios; (4) a separate consideration of the

broad and narrow line regions, whereas this distinction was ignored in the above studies of NGC 4151; and (5) a comparison of results for objects representing opposite extremes of the observed Seyfert galaxy spectral types.

The last point is particularly important in relation to the most recent studies of QSO's. MacAlpine considered a model aimed at agreement with the spectrum of 3C 273 and presented a comprehensive study of the effect of model parameter changes but made little application to specific objects. Davidson (1972) attempted to fit a composite spectrum found by combining the observations of several QSO's before analysis. In contrast, the present work analyzes two individual Seyfert galaxies having substantially different spectra with the aim of understanding the differences as well as the similarities.

Chapter II briefly reviews the basic physical processes that are important in the models. Chapter III discusses the observations and models of NGC 1068, and Chapter IV discusses 3C 120. The conclusions and suggestions for further work are summarized in Chapter V. Finally, the computer program used to calculate the models is described in the Appendix.

II. STRUCTURE OF PHOTOIONIZED NEBULAE

(A) Physical processes

The subject of the physical processes in photoionized nebulae, as used in the models in this thesis, is adequately discussed in the literature (e.g., Seaton 1960; MacAlpine 1971, 1972; and references cited therein). This section lists some of the basic equations for convenience. The problem is to determine the temperature and state of ionization in the nebula, given assumptions about the ionizing radiation spectrum and the density, location, and chemical composition of the gas. The usual analysis assumes a steady state in which the electrons have a Maxwellian velocity distribution characterized by an electron temperature T. The degree of ionization of any element Z is determined by equating the rate (cm^{-3} s^{-1}) at which each ionic species Z^z (element Z missing z electrons) is destroyed by ionization to the rate at which it is formed by recombination. The temperature is such that energy is absorbed from the radiation field at the same rate (ergs cm^{-3} s^{-1}) as it is carried away by radiation originating at the point in question. The observable properties of the hypothetical nebula, such as the emission line luminosities (ergs s^{-1}), are given by volume integrals over the nebula.

Ionization may result from the action of the radiation field, from electron impact, and in some cases from charge transfer. The probability per second that Z^z will be photoionized is

$$\Gamma_p(Z^z) = \int_{\nu_i}^{\infty} a_\nu f_\nu (h\nu)^{-1} d\nu, \qquad \text{II-1}$$

where f_ν is the radiation flux density in ergs cm^{-2} s^{-1} Hz^{-1}, a_ν is the photoionization cross-section in cm^2, and $h\nu_i = I(Z^z)$ is the ionization potential. Given a point source of radiation and spherical symmetry, the radiation field consists of a contribution from the primary source $f_\nu^p = L_\nu e^{-\tau\nu}(4\pi R^2)^{-1}$, where τ_ν is the optical depth at R, and a contribution of diffuse (secondary) radiation created by the ionized gas, $f_\nu^s = cu_\nu^s$, where u_ν^s is the diffuse spectral energy density (ergs cm^{-3} Hz^{-1}). If several electron shells are important, then the contributions of each must be added. The collisional ionization probability is

$$\Gamma_c(Z^z) = 1.3\times10^{-8}\xi' T^{1/2} F(Z^z) N_e e^{-I'/kT}, \qquad \text{II-2}$$

where ξ' is the effective number of outer shell electrons, I' is the effective ionization potential, T is in degrees Kelvin, and the collisional focusing factor F is of order unity and has the value 1.4 for H^0 (Cox and Tucker 1969).

The probability per second of radiative electron capture by Z^{z+1} to form Z^z is

$$\Gamma_r(Z^{z+1}) = \alpha(Z^z,T)N_e, \qquad \text{II-3}$$

where $\alpha \equiv \sum_{n=1}^{\infty}\alpha_n$ and α_n is the radiative recombination coefficient ($cm^3\ s^{-1}$) to level n. (The process of dielectronic recombination was ignored because it is not of major importance for the models discussed here.) For a steady state, the ionization is given by

$$Y(Z^z) \equiv N(Z^{z+1})/N(Z^z) = \frac{\Gamma_p(Z^z) + C(Z^z,T)N_e}{\alpha(Z^z,T)N_e}, \qquad \text{II-4}$$

where $N(Z^z)$ is the number of ions per cm^3, and $C(Z^z,T)$ is the coefficient of N_e in equation (II-2). Given $Y(Z^z)$ for all ions of an element, the fractional abundances $X(Z^z) \equiv N(Z^z)/N(Z)$ are easily calculated. The electron density is then given by

$$N_e = \sum_{Z,z} zN(Z^z). \qquad \text{II-5}$$

The diffuse radiation consists mainly of Lyman continuum and Lyman line radiation from recombining hydrogen and helium. The ionizing Lyman line radiation was assumed to be absorbed "on-the-spot" (OS) by hydrogen and helium; the Lyman continuum usually was assumed to be absorbed OS in the case of H^0 and He^+ and ignored in the case of He^0. The OS approximation for the Lyman continuum is incorporated into equation (II-4) by omitting the Lyc contribution to the ionization rate and replacing

α by $\alpha_B \equiv \alpha - \alpha_1$.

At the temperatures of interest here ($T \approx 10^{4}$° K), the oxygen charge transfer reaction $O^+ + H^0 \rightleftarrows O^0 + H^+$ occurs fast enough that

$$Y(O^0) = 8/9\ Y(H^0) \qquad \text{II-6a}$$

(Brown 1972). For nitrogen, Steigman, Werner, and Geldon (1971) have found that at these temperatures

$$Y(N^0) = 4.5\ Y(H^0), \qquad \text{II-6b}$$

even though the energy defect for the H,N reaction is quite large.

The equilibrium electron temperature of the ionized gas may be found from equivalent formulations of the problem in terms of the radiation absorbed and emitted by the gas, or in terms of the kinetic energy gained and lost by the electron ensemble. The kinetic energy given to the photoelectrons ejected from Z^z (ergs cm^{-3} s^{-1}) is

$$G(Z^z) = N(Z^z) \int_{\nu_i}^{\infty} f_\nu a_\nu (1-\nu_i/\nu) d\nu, \qquad \text{II-7}$$

where a summation over contributions from inner (filled) electron shells may be required. The total energy gain G is found by adding the contribution from all ions. Heating due to scattering of the primary radiation by free electrons was included in the models but was never important.

In a steady state, the energy gain G equals the loss

L resulting from radiative recombination, thermal bremmstrahlung, collisional ionization, and collisional line emission. The kinetic energy lost per second per cm^3 by electrons recombining to form Z^z is

$$L_r = \beta(Z^z)kTN_eN(Z^{z+1}). \qquad \text{II-8}$$

The ratio β/α is the mean kinetic energy of the recombining electrons in units of kT, and it has the value ~ 0.8 for $T \simeq 10^{4\circ}$ K (Seaton 1959). The total recombination kinetic energy loss L_r is found by summing equation (II-8) for all ions. The assumed OS absorption of the diffuse hydrogen and helium Lyman continuum can be accounted for by the use of a reduced thermal emission coefficient $\beta_B(Z^z)$. A further kinetic energy loss due to collisional ionization is

$$L_c = \sum_{Z,z} I(Z^z)N(Z^z)\Gamma_c(Z^z). \qquad \text{II-9}$$

The rate of energy loss due to thermal bremsstrahlung by Z^z is

$$L_B(Z^z) = 1.42\times10^{-27}T^{1/2}N_eN(Z^{z+1})z^2g_B(\lambda), \qquad \text{II-10}$$

where g_B is the integrated bremsstrahlung gaunt factor, $\lambda \equiv z^2I(H^0)/kT = 15.8z^2/T_4$, and $T_4 \equiv T/10^{4\circ}$ K. Karzas and Latter (1961) give a graph of the function g_B, and in most cases an adequate approximation is $g_B \simeq 1.4$.

Collisional excitation followed by radiative decay usually provides the largest kinetic energy loss. For forbidden lines, the radiative and collisional transition probabilities are often comparable, and the steady state equations for the energy level populations may be solved as described by Seaton (1960). This involves computation of the relevant probabilities for collisional deactivation from level u to level l,

$$d_{ul} = 8.63\times10^{-6} N_e T^{-1/2} \Omega(l,u)/g_u \quad s^{-1}, \qquad \text{II-11}$$

and for collisional excitation

$$d_{lu} = d_{ul}(g_u/g_l)\exp(-E_{lu}/kT), \qquad \text{II-12}$$

where g_i is the statistical weight of level i, $\Omega(l,u)$ is the dimensionless collision strength, and E_{lu} is the energy difference between the two levels. Given the excited state populations, the emissivity in a line of wavelength λ is

$$4\pi j(\lambda) = A_{ul} E_{lu} N(Z^z,u) \quad \text{ergs cm}^{-3}\ \text{s}^{-1}, \qquad \text{II-13}$$

where A_{ul} is the spontaneous transition probability. For permitted lines and for forbidden lines where the electron density is low, $A_{ul} >> d_{ul}$. In this case, the emissivity is

$$4\pi j(\lambda) = d_{lu} E_{lu} B(\lambda) N(Z^z), \qquad \text{II-14}$$

where the branching ratio B is the probability that an ion in the excited state u will make the transition to level l rather than some other transition.

Line and continuum emission due to radiative recombination are also of observational interest. For recombination lines, the emissivity is

$$4\pi j(\lambda) = \alpha_{ul}(Z^z,T)N_e N(Z^{z+1})E_{lu}. \qquad \text{II-15}$$

The effective recombination coefficients α_{ul} for H I, He I, and He II are given by Brocklehurst (1971, 1972). Continuum emission features, such as the Balmer Jump, can be calculated with the aid of continuum emission coefficients (Brown and Mathews 1970) defined so that

$$4\pi j_\nu(Z^z) = \gamma_\nu(Z^z,T)N_e N(Z^{z+1}), \qquad \text{II-16}$$

where j_ν is in ergs cm^{-3} s^{-1} Hz^{-1} $ster^{-1}$.

To calculate the emission from a model nebula, it is necessary to solve the ionization and thermal equilibrium equations along with the optical depth equation

$$d\tau_\nu/dr = \sum_{Z,z} a_\nu(Z^z)N(Z^z). \qquad \text{II-17}$$

The emission line luminosities are then found by integrating the emissivity over the volume of the nebula,

$$L(\lambda) = \int_V 4\pi j(\lambda) d^3\hat{r}, \qquad \text{II-18}$$

provided that the nebula is optically thin in the lines.

(B) Ionization structure

The ionization structure of conventional models of H II regions is governed by the depletion of the primary ionizing flux of photons by photoionization of hydrogen and helium. Under the conditions usually assumed, the flux of ionizing radiation is strong enough that hydrogen is almost completely ionized from the center of the nebula out to the radius $R(H^+)$ at which all the ionizing photons have been used up. Beyond this Strömgren sphere, the ionization drops abruptly to near zero. For normal helium abundances and ionizing radiation spectra, the photons capable of ionizing He^+ are used up within an He^+ Strömgren sphere well inside $R(H^+)$. In this case, the ionization of hydrogen and helium defines three zones: (1) an inner region, bounded by $R(He^{++})$, in which helium is mostly He^{++} and hydrogen is mostly H^+; (2) an He^+, H^+ region between $R(He^{++})$ and $R(H^+)$; and (3) an outer H^0 region. Of the heavier elements, zone (1) may contain fairly highly ionized species such as O^{+5} and Ne^{+4}; zone (2) contains important ions such as C^{+3}, O^{+2}, and Ne^{+2}; and zone (3) contains C^+, O^0, Mg^+, and S^+.

This picture fails if the gas is only partially ionized even where τ_ν is small. The condition for nearly

complete ionization within the Strömgren sphere is that $L_\nu/4\pi R^2 N$ be large enough that $\Gamma_p(Z^z) >> \Gamma_r(Z^{z+1})$ for the ions of interest. Let us consider hydrogen in the vicinity of a source of ionizing radiation of power law form, $L_\nu = L_o(\nu/\nu_o)^\alpha$, where ν_o = 1 Ryd. Then from equation (II-1) we find

$$\Gamma_p = L_o a_o [4\pi R^2 h(3-\alpha)]^{-1}, \qquad \text{II-19}$$

where $a_o = a_{\nu_o}(H^0) = 6.3 \times 10^{-18}$ cm^2. We have assumed that τ_ν is small and we have used the approximation that $a_\nu = a_o(\nu/\nu_o)^{-3}$. For $T_4 \approx 1$, we then find from equation (II-4) that

$$Y(H^0) \approx 3 \times 10^5 L_{29}[(3-\alpha) R_{20}{}^2 N_4]^{-1}, \qquad \text{II-20}$$

where $L_{29} = L_o/10^{29}$ ergs s^{-1} Hz^{-1}, $N_4 = N_e/10^4$ cm^{-3}, and $R_{20} = R/10^{20}$ cm. Thus for $L_{29} = 1$, R = 10 pc, we find that $Y(H^0) \approx 10^6/N_4$, and hence hydrogen is highly ionized as long as the density is less than about 10^9 cm^{-3}. This condition is clearly satisfied in the forbidden line regions in Seyfert nuclei. The permitted line regions have $N > 10^8$ cm^{-3}, so that it is possible that they are only partially ionized.

Given nearly complete ionization of hydrogen inside the Strömgren sphere, we may estimate its size from the condition that nearly all of the ionizing photons are

absorbed by hydrogen. Then in a steady state, the number of primary ionizing photons emitted per second, $Q(H^0)$, equals the number of recombinations to excited states of H^0 throughout the nebula. This leads to the equation

$$\int_{\nu_0}^{\infty} L_\nu d\nu/h\nu = 4/3\ \pi R(H^+)^3 \alpha_B(H^0,T) N^2. \qquad \text{II-21}$$

A similar equation applies to $R(He^{++})$ if the helium abundance is large enough that nearly all photons with $\nu>4$ Ryd are absorbed by He^+. For $L_\nu \propto \nu^\alpha$, with $\alpha<0$, we then find

$$[R(He^{++})/R(H^+)]^3 \simeq (4^\alpha/6) N(H)/N(He), \qquad \text{II-22}$$

where we have used $\alpha_B(He^+)/\alpha_B(H^0) \simeq 6$. For $\alpha = -1$, we see that $R(He^{++})/R(H^+) < 1$ for $N(He)/N(H) \gtrsim 0.04$. Thus for normal helium abundances, most photons with $\nu>4$ Ryd are absorbed by He^+. Therefore, the relative He II and H I recombination line intensities are determined by the slope of the ionizing radiation spectrum and not by the helium abundance (Williams 1971). In this case, we have

$$I(\lambda 4686)/I(H\beta) \simeq 2.5\times 4^\alpha, \qquad \text{II-23}$$

where 2.5 is the value of the ratio $[\alpha(\lambda 4686)/\alpha_B(He^+)]/[\alpha(H\beta)/\alpha_B(H^0)]$. A weaker $\lambda 4686$ line would imply either that the helium abundance was quite low or that the conditions were not as assumed (e.g., the ionization was

low due to a high gas density).

Bahcall and Kozlovsky (1969) calculated models of 3C 273 in which they found $\alpha \simeq -0.7$ was necessary to provide enough high frequency photons to explain the strengths of the lines of the heavy elements such as C IV. By equation (II-23), a normal helium abundance would then result in $I(\lambda 4686)/I(H\beta) \simeq 1$, but this value greatly exceeds the observational upper limit. Thus Bahcall and Kozlovsky inferred that the helium abundance is very small in 3C 273.

Except for $\alpha << -1$ or for $N(He)/N(H) \gtrsim 0.3$, helium is singly ionized throughout the region between $R(He^{++})$ and $R(H^{+})$. This leads to the equation

$$I(\lambda 5876)/I(H\beta) \simeq 1.3[N(He)/N(H)][1-R(He^{++})^3/R(H^{+})^3]. \qquad \text{II-24}$$

The helium abundance in this case is given by

$$\frac{N(He)}{N(H)} \simeq \frac{I(\lambda 4686)\alpha(H\beta)}{I(H\beta)\alpha(\lambda 4686)} + \frac{I(\lambda 5876)\alpha(H\beta)}{I(H\beta)\alpha(\lambda 5876)}$$

$$\simeq 0.086 I(\lambda 4686)/I(H\beta) + 0.74 I(\lambda 5876)/I(H\beta). \qquad \text{II-25}$$

(C) Scale transformations

There are some changes in the luminosity, radius, and density of a model nebula which do not change the ionization structure and relative emission line intensities. An appreciation of these relations facilitates both the study of individual objects and the comparison of models for different objects. We shall consider three general classes of scale transformations: (1) strict homologies relating models with luminosity and radius varying so as to keep L/R^2 the same; (2) transformations in which the gas density, luminosity, and radius change so that L/NR^2 remains the same; and (3) the weakest class of transformations, in which L/NR^2 changes but the Strömgren sphere structure, governed by the shape of the ionizing radiation spectrum, remains roughly similar.

The most obvious strict homology relates models in which a point source of radiation L ionizes a thin shell of gas at radius R. If the luminsoity is increased by a factor A, $L \rightarrow AL$, and the radius of the shell is increased by the factor $A^{1/2}$, $R \rightarrow A^{1/2}R$, then the flux density incident on the shell, $f = L/4\pi R^2$, is unchanged. Thus the ionization structure, which is essentially plane-parallel, is unchanged; and all emission line and continuum intensity ratios are the same. For filamentary models

with volume filling factor f, the corresponding homology is $L \rightarrow AL$, $f \rightarrow A^{-1/2}f$. The radius $R(\tau_\nu)$ at which τ_ν has a particular value scales as $R \rightarrow A^{1/2}R$, since $d\tau_\nu \propto NdR$. This is exactly the R transformation required to preserve the flux density $f_\nu = L_\nu(4\pi R^2)^{-1}\exp(-\tau_\nu)$, which is necessary to keep the ionization and thus the opacity the same at $R(\tau_\nu)$. This consistency assures that the transformation is fact yields an exactly similar family of models with identical relative line strengths.

Another class of scale transformations involves a change in the gas density. Such models are not strictly homologous because the collisional suppression of forbidden lines is density dependent. However, the resulting temperature change has little effect on the ionization structure and permitted line strengths. This is a result of the fact that the recombination coefficients are less sensitive to the temperature than are the collisional excitation rates. In the case of a uniform ball of gas, the transformation is $L \rightarrow AL$, $N \rightarrow A^{-1}N$. To preserve the correct optical depths, we require $R \rightarrow AR$, so that the product NdR remains unchanged; and this is just what is required to keep $Y(Z^z) \propto L_\nu(NR^2)^{-1}\exp(-\tau_\nu)$ the same. Note that a thick shell transforms in the same way provided that the inner and outer boundaries are scaled as $R_b \rightarrow AR_b$. For a ball of filaments, the transformation at constant luminosity is $N \rightarrow BN$, $f \rightarrow B^{-1/2}f$. For a thin

shell, there is more freedom, since this is essentially a plane-parallel problem in which the ratio L/NR^2_{shell} determines the ionization, and the thickness of the ionization zones need not scale as R_{shell}. For example, the transformation L→AL, N→AN, and R_{shell} = const. belongs to this class. All of the above transformations can be proved using the ionization structure equations, although for class (2) it is necessary to assume that the temperature is unaffected by collisional deactivation of ions.

Finally, the third class of transformations is based on equation (II-22), which states that under the right conditions the relative volumes of the major ionization zones are determined by the frequency distribution of the ionizing radiation. Thus the ratios of the intensities of the lines of the dominant ions in these zones depend weakly on the other model parameters, given fixed chemical abundances. These lines include Hβ, He I λ5876, He II λ4686, C IV λ1549, [O III] λ5007, and [Ne III] λ3869.

III. NGC 1068

NGC 1068 is a large Sb spiral galaxy whose photograph is contained in The Hubble Atlas of Galaxies (Sandage 1961) as an example of a galaxy with a marked contrast in surface brightness between the inner and outer portions of the disk. The Seyfert nucleus shows time variations in brightness around an average $m_B = 11^m.8$. The redshift is $z = 0.0036$. The strongest emission lines from the nucleus are [O III] λ5007, [N II] λ6583, and Hα. Other strong lines, having intensities in the range ∿5-10 percent of the [O III] lines, include He I λ10830, He II λ4686, [O II] λ3727 and λ7325, [Ne III] λ3869, [Ne V] λ3426, [S II] λ4072 and λ6720, and [S III] λ9532. Spectrograms show that the Seyfert nucleus is at least partially resolved on a scale of a few seconds of arc. Thus at least some of the line emission comes from a region roughly 100 pc across. Time variations of the nonstellar continuum show that the diameter of the continuum source is less than about one light-year. Rapid mass motions at velocities up to 600 km s^{-1} have been observed in clouds near the nucleus (Walker 1968), and similar velocities are indicated by the structure of the line profiles of the nucleus. Figure 1 summarizes the observations of NGC 1068 in the radio to X-ray fre-

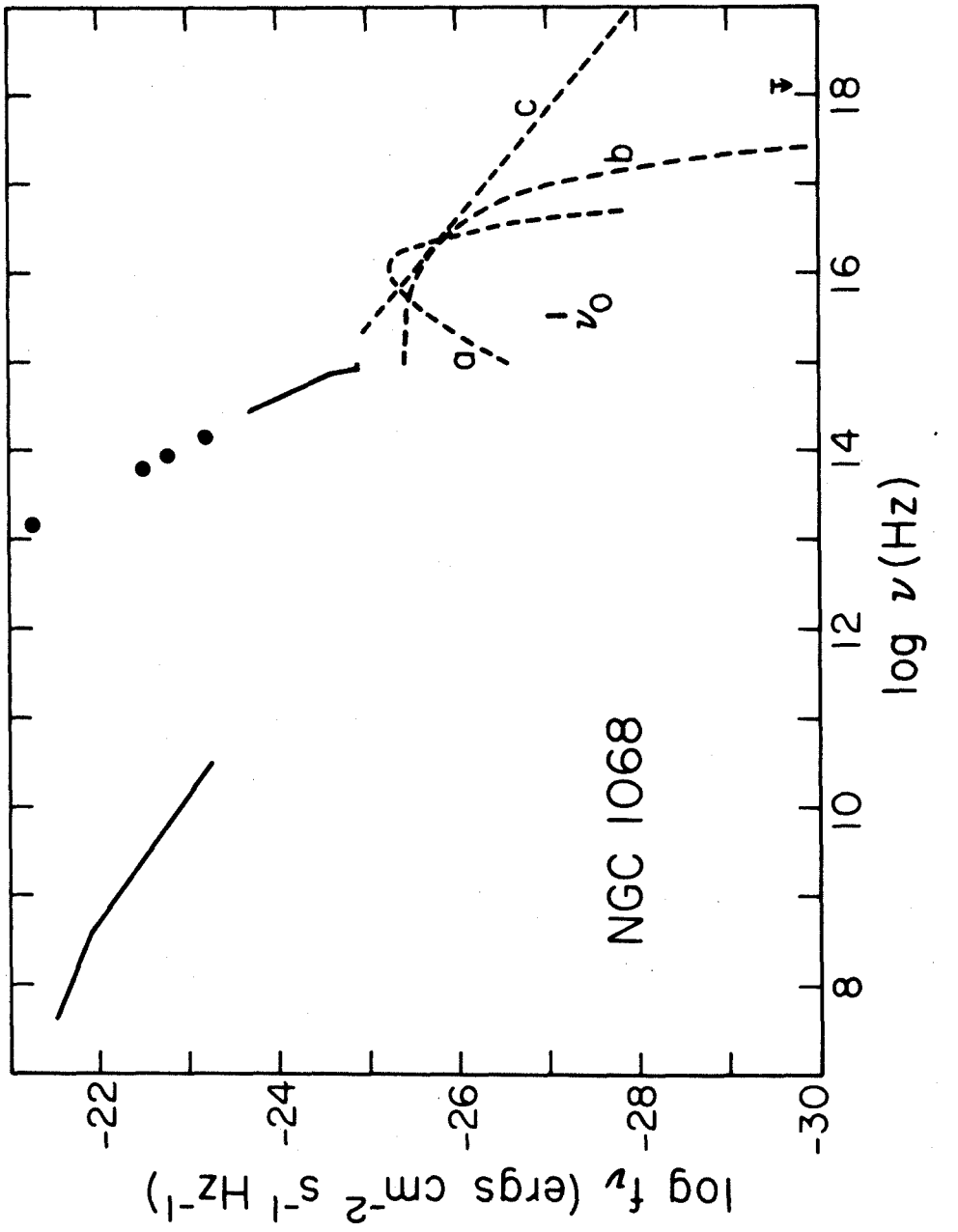

Fig. 1. - Observations of NGC 1068 from Kellermann and Pauliny-Toth (1971), Rieke and Low (1972), Shields and Oke (1972), and Kellogg (1972). The dashed curves show the ionizing continua assumed in (a) Models 1, 2, and 3; (b) Model 4; and (c) Model 5.

quency range.

(A) Observations

Observations of the nucleus of NGC 1068 were made by Professor J. B. Oke and the author on the night of 1971 July 28/29 with the multichannel photoelectric spectrometer attached to the 200-inch telescope (Oke 1969). The wavelength interval λλ3300-11090 was covered with a bandpass of 20 A at intervals of 10 A for λ<5790 A and 20 A for λ>5790A. The entrance aperature had a diameter corresponding to 7" on the sky, and the sky background and dark count were removed by subtracting the signal in another 7" aperature 40" away. The small amount of starlight in the reference aperture diminished slightly the stellar contribution measured from the nucleus, but this does not affect the emission line intensities. Further observations were made on the night of 1971 November 9/10 to fill several small gaps in the wavelength coverage. The fluxes were reduced to outside the earth's atmosphere according to the absolute calibration of α Lyrae by Oke and Schild (1969). In addition to the photoelectric observations, we have obtained several coudé spectrograms of the nucleus of NGC 1068 with the 200-inch telescope. These show that some of the broad line emission comes from a region ∿1"-2" across.

Table 1 lists the emission line fluxes determined from the photoelectric observations. The separation of Hα from [N II] λλ6548, 6583 was made using the results of Eilek et al. (1972), which indicate that I(λλ6548, 6583)/I(Hα) = 2.0. This value is consistent with our coudé spectrogram, which shows that λ6583 is somewhat stronger than Hα.

Wampler (1971) has shown that interstellar reddening occurs in or near the nuclei of several Seyfert galaxies, including NGC 1068. According to our data, there is good agreement between the amount of reddening indicated by the Balmer decrement and by the [S II] line ratio I(λ10320)/I(λ4072), which should have a value near 0.52 (Miller 1968). We have adopted a value for the extinction of $A_V = 1^m.3$, based on the reddening function given by Seaton (1960). This amount of reddening agrees with that found by Wampler (1971). The reddening corrected line intensities are given in Table 1.

The agreement of the reddening inferred from the Balmer decrement and the [S II] ratio is interesting for two reasons. First, it suggests that the reddening is uniform and occurs outside the emission line region. Second, there is now no direct observational evidence for an anomalously steep Balmer decrement that might result from collisional excitation or self-absorption of

TABLE 1

EMISSION LINE INTENSITIES OF THE NGC 1068

Ion	λ	F(λ)† (10^{-13} ergs cm^{-2} s^{-1})	I(λ)* corrected for reddening
He I	10830	53	1.0
[S II]	10320	6:	0.12:
P 8	9546	39	0.87
[S III]	9532		
[S III]	9069	14	0.32
[A III]	7751	1.0:	0.03:
[O II]	7325	4:	0.12:
[A III]	7136	4.4	0.15
He I	7065	0.9:	0.03:
[S II]	6720	17	0.63
[N II]	6583	137	5.2
H α	6563	69	2.6
[O I]	6364	1.3:	0.05:
[O I]	6300	7	0.29
[Fe VII]	6086	2.8	0.12
He I	5876	1.8:	0.08:
[N II]	5755	2.4	0.11
[Fe VII	5721	0.8:	0.04:
[N I]	5199	0.8:	0.04:
[Fe VII]	5158	0.9:	0.05:
[O III]	5007	218	13.1
[O III]	4959		
H β	4861	15.4	1.00
He II	4686	7	0.5
[O III]	4363	1.4:	0.11:
H γ	4340	4:	0.3:
H δ	4101	3.0	0.26
[S II]	4072	3.5	0.31
[Ne III]	3968	4	0.35
[Ne III]	3869	11	1.05
[Fe VII]	3760	2:	0.21:
[O II]	3727	10	1.02
[Ne V]	3426	16	1.68
[Ne V]	3346	4.2	0.45

*Relative to Hβ. $L(H\beta) = 3.0 \times 10^{41}$ ergs s^{-1}

†Colon indicates uncertainty of 50 percent or more.

the Balmer lines.

(B) Comparison of NGC 1068 and NGC 7027

Seyfert (1943) compared the spectrum of the high excitation planetary nebula NGC 7027 to the spectrum of NGC 1068. He remarked, "The intensities of the lines are similar to those in the planetary nebula NGC 7027 except that the [O II], [S II], [N I], and [Fe VII] lines are considerably stronger in NGC 1068." The main point of this chapter is to show that this comparison in physically meaningful, and to see what information can be derived from an analysis of the similarities and differences between the spectra of NGC 1068 and NGC 7027.

Table 2 compares the reddening corrected emission line intensities of NGC 1068 and NGC 7027, normalized to Hβ. The intensities of multiplets have been added, as will be done throughout this thesis; for example, I(λ9532) means I(λ9069) + I(λ9532). The data on NGC 1068 are from Table 1; and the data on NGC 7027 are from Miller and Mathews (1972), O'Dell (1963), and Aller et al. (1963). The striking pattern displayed by Table 2 is that with the exception of [Fe VII], the high excitation lines (defined here as the recombination lines of hydrogen and helium and the forbidden lines of atoms twice or more ionized) agree to within ∿30 percent, whereas the

TABLE 2

COMPARISON OF NGC 1068 and NGC 7027*

Ion	λ	I(1068)	I(7027)	$\frac{I(1068)}{I(7027)}$
[Ne V]	3426	2.13	1.93	1.1
He II	4686	0.5	0.49	1.0
[O III]	4363	0.11:	0.25	0.4:
[O III]	5007	13.1	18.6	0.7
[Ne III]	3869	1.40	1.70	0.8
H β	4861	1.00	1.00	1.0
He I	5876	0.08:	0.11	0.7:
[S III]	9532	1.19	1.41	0.85
[A III]	7136	0.20	0.27	0.7
[N II]	5755	0.11	0.06	1.8
[N II]	6583	5.2	1.26	4.1
[O II]	7325	0.12	0.32	0.4
[O II]	3727	1.02	0.35	2.9
[S II]	4072	0.31	0.16	2.0
[S II]	6720	0.63	0.062	10
[N I]	5199	0.05:	0.009:	5:
[O I]	6300	0.34	0.17	2.0

*Reddening corrected emission line intensities relative to Hβ.

low excitation lines (forbidden lines of neutral or once ionized atoms) differ by at least a factor of two and as much as a factor of ten. Except for [O II] λ7325, the low excitation lines are much stronger in NGC 1068.

The case of [Fe VII] deserves special attention, since it is the one exception to the good agreement of the high excitation lines. Although the data for these weak lines are uncertain, they do indicate that the [Fe VII] lines are several times as intense in NGC 1068 as in NGC 7027. Since my computer models do not include iron, I do not have detailed information on this point. However, the closeness of the ionization potentials of Ne^{+4} and Fe^{+6}, along with their neighbor ions, suggests that these ions are likely to occur together, regardless of the ionization model adopted. Thus we shall assume that the greater strength of the [Fe VII] lines in NGC 1068 is due to a larger abundance of iron. It would be interesting to see whether there is evidence for an over-abundance of iron outside the nucleus of NGC 1068.

The close agreement of the high excitation line intensities of NGC 1068 and NGC 7027 suggests that a simple model may provide an explanation not only of this agreement but also of the actual values of the line intensities. On the other hand, there is no comparable simplicity in the case of the low excitation lines, and

hence a simple quantitative explanation of these seems less likely. Thus the fundamental problem posed by the observations is to explain in a natural way the values of and the agreement between the high excitation line intensities and the disagreement of the low excitation line intensities. The purpose of the next section is to show that photoionization by an ultraviolet continuum provides this explanation. This will be done by showing (1) that a simple model for the high excitation region can explain the high excitation line intensities of NGC 7027, (2) that this model can be transformed to the scale of NGC 1068, and (3) that another component (low excitation region) must be added to the model to explain the low excitation lines.

(C) The high excitation region

(1) A model of NGC 7027

We begin by considering a model of NGC 7027 in which the ionizing radiation is described by the Planck function

$$L = L_o(\nu/\nu_o)^3 \frac{\exp(h\nu_o/kT_b)-1}{\exp(h\nu/kT_b)-1}, \qquad \text{III-1}$$

where ν_o = 1 Ryd. Although black-body radiation is not an accurate approximation to the radiation from a hot star, the differences are not important to the present

discussion. The main reason is that at a given temperature in the range of interest, black-body and model atmosphere fluxes (Hummer and Mihalas 1970) have nearly the same relative numbers of H^0 and He^+ ionizing photons.

The computer program described in the Appendix was used to calculate models with several values of T_b and L_o, and adequate agreement with L(λ4686) and L(Hβ) was obtained for T_b = 175,000° K and $L_o = 0.9 \times 10^{21}$ ergs s^{-1} Hz^{-1}. The heavy element abundances (see Table 3) were the same as those used by MacAlpine (1972) except that iron and silicon were not included. The helium abundance N(He)/N(H) = 0.127 was taken from Miller and Mathews (1972) and was roughly confirmed by the results. For the gas density and filamentary volume filling factor, the values $N = 6 \times 10^4$ cm^{-3} and f = 0.04 also were taken from Miller and Mathews. The line intensities in this model (Model 1) are given in Table 4, and the factional ionization, electron temperature, and electron density are shown in Figures 2-4.

The agreement with the observations is quite good for the high excitation lines. The largest discrepancy is that [Ne III] and [Ne V] are about 35 percent too weak, and this can be corrected by a small increase of the neon abundance. Model 1 has I(λ5007)/I(Hβ) and I(λ5007)/I(λ4363) slightly too large. A higher electron

TABLE 3

CHEMICAL ABUNDANCES USED IN THE MODELS*

Element	N(Z)/N(H)	Highest ion considered
H	1.00	H^{+}
C	3.5×10^{-4}	C^{+6}
N	1.3×10^{-4}	N^{+7}
O	7.9×10^{-4}	O^{+8}
Ne	7.9×10^{-5}	Ne^{+6}
Mg	2.5×10^{-5}	Mg^{+8}
S	7.9×10^{-5}	S^{+5}

*Adopted from MacAlpine (1972).

TABLE 4

EMISSION LINE INTENSITIES IN MODELS 1, 2, and 3.*

Ion	λ	Model 2 ($N=6\times10^3$)	Model 1 ($N=6\times10^4$)	Model 3 ($N=6\times10^5$)
[Ne V]	3426	1.2	1.4	0.3
He II	4686	0.6	0.6	0.5
[O III]	4363	0.32	0.29	0.32
[O III]	5007	35	24	18
[Ne III]	3869	1.8	1.0	1.4
[S III]	9532	0.09	1.0	6.3
H β	4861	1.0	1.0	1.0
He I	5876	0.11	0.12	0.18
[N II]	5755	0.0005	0.006	0.05
[N II]	6583	0.04	0.25	0.79
[O II]	7325	0.006	0.049	0.21
[O III]	3727	0.011	0.011	0.009
[S II]	4072	0.001	0.017	0.72
[S II]	6720	0.005	0.091	0.87
[O I]	6300	0.014	0.19	2.3

*Ionized by black body radiation at 1.75×10^{5}° K.

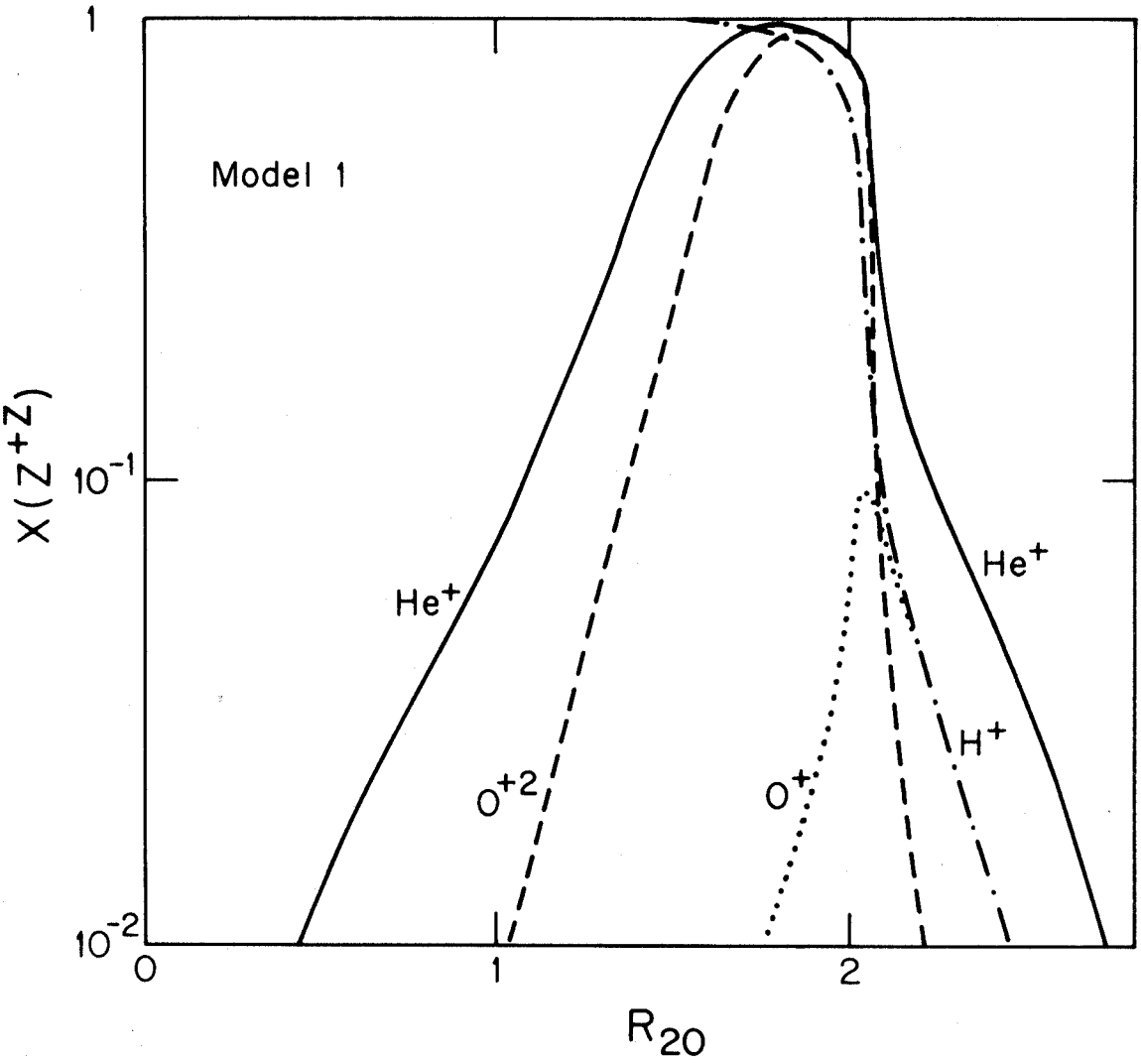

Fig. 2. - Ionization of hydrogen, helium, and oxygen in Model 1. The radial scale (units of 10^{20} cm) applies to NGC 1068. Note that charge exchange removes O^+ from the H^0 zone.

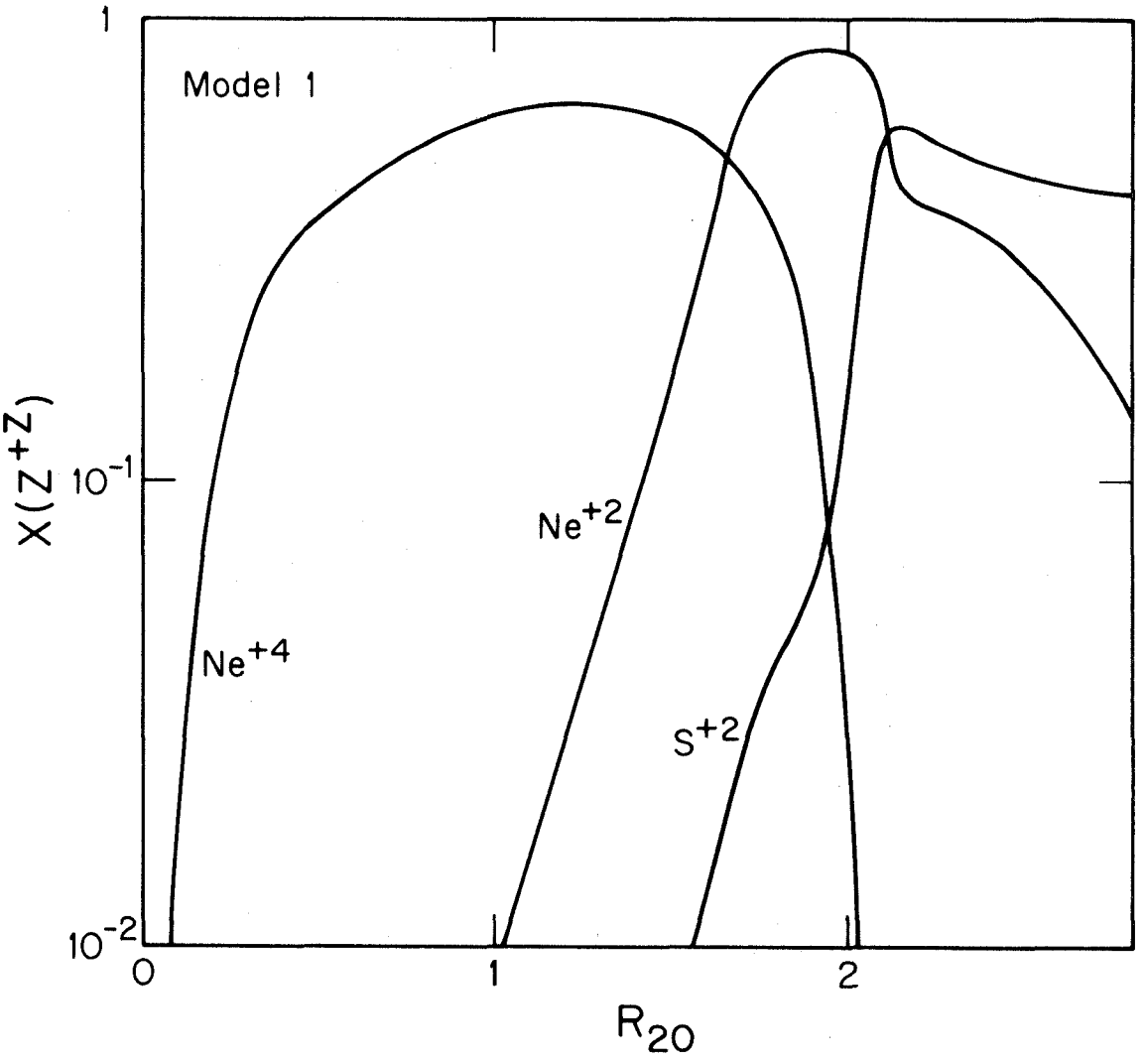

Fig. 3. - Ionization of neon and sulphur in Model 1.

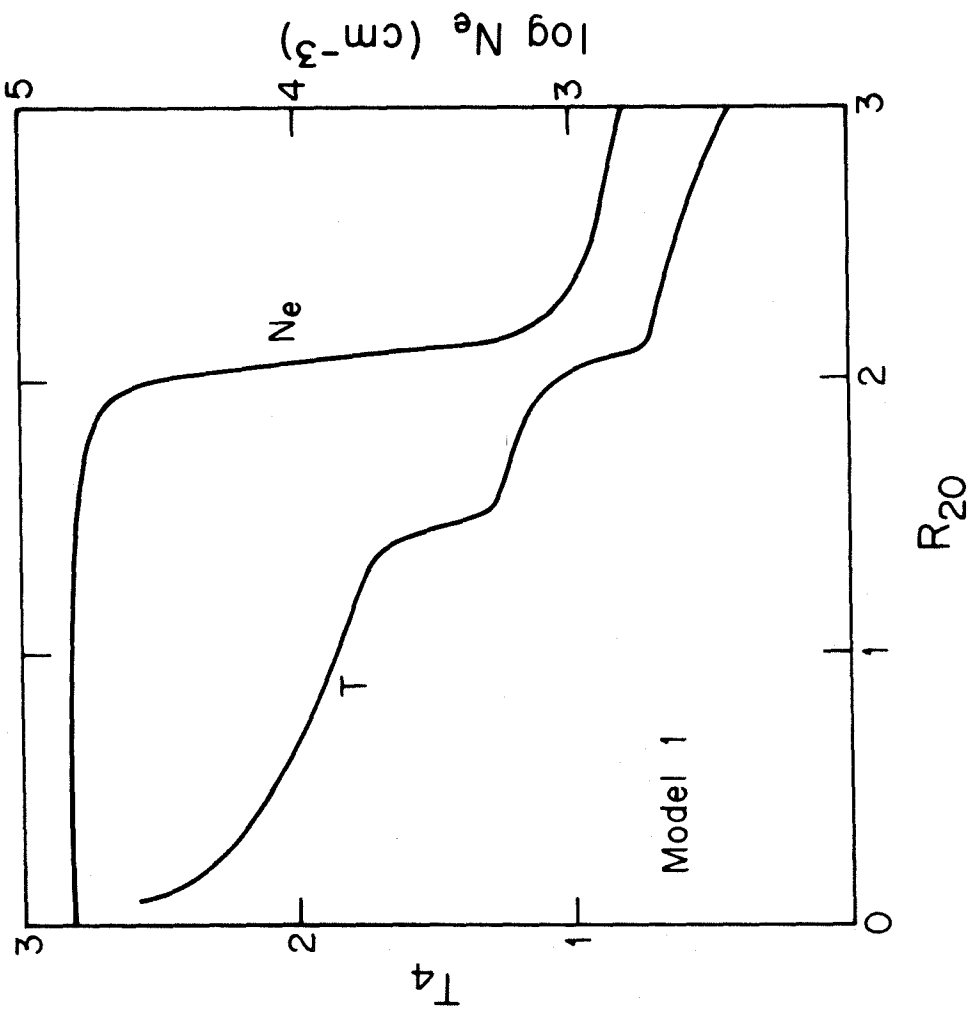

Fig. 4. - Electron temperature and density in Model 1. The temperature drops at $R(He^{++})$ and $R(H^+)$.

temperature would reduce I(λ5007)/I(λ4363) but would increase I(λ5007)/I(Hβ). Moreover, additional models have shown that it is difficult to achieve a sufficiently higher temperature by modifying the gas density or ionizing radiation spectrum. A reduced oxygen abundance would lead to a smaller I(λ5007)/I(Hβ), but the temperature increase resulting from the required abundance reduction is much too small to account for the observed value of I(λ5007)/I(λ4363). The most likely remaining explanation is that some of the gas in NGC 7027 has $N_e \gtrsim 10^6$ cm^{-3}, so that there is some collisional suppression of λ5007.

In contrast to the good agreement for the high excitation lines, Model 1 yields very poor agreement for the low excitation lines, most of which are much too weak. This is in accord with the expectation reached by comparing the spectra of NGC 1068 and NGC 7027.

(2) Application to NGC 1068

We now show that Model 1, which accounts for the high excitation lines of NGC 7027, is applicable to NGC 1068 as well. Taking L(Hβ) as a measure of the luminosity of the nebulae, we find L(NGC 1068)/L(NGC 7027) = 3.0×10^{41} ergs s^{-1}/2.5×10^{35} ergs s^{-1} = 1.2×10^6. The ionizing continua must have nearly the same luminosity ratio.

The average angular size of NGC 7027 is about 8" (from the data of Perek and Khoutek [1967]), which corresponds to R = 0.09 pc at a distance of 1.77 kpc (O'Dell 1962). Taking an angular radius of 1" for the Seyfert nucleus of NGC 1068, and a distance of 22 Mpc deduced from z = 0.0036 and H = 50 km s^{-1}, we find R = 100 pc. The ratio of the ionizing continuum flux densities at corresponding points in the two nebulae is therefore $f_\nu(1068)/f_\nu(7027) = [L_\nu(1068)/L_\nu(7027)]/[R(1068)/R(7027)]^2 = 1.0$. The fact that this ratio is unity means that an exact homology relates similar models of the two objects, as discussed in §II-C. In the case of Model 1, the transformation is achieved by substituting $L_o(1068) = 1.2\times10^6 L_o(7027) = 1.1\times10^{27}$ ergs s^{-1} Hz^{-1} and $f(1068) = (1.2\times10^6)^{-1/2} f(7027) = 3.7\times10^{-5}$. Thus Model 1 is applicable to NGC 1068, and henceforth the term "Model 1" will refer to this model on either scale.

The above transformation does not depend on the distance to either object, since the essential property is that the reddening corrected surface brightness is the same for both nebulae. Furthermore, small deviations from the strict homology do not destroy the validity of applying Model 1 to NGC 1068. Small differences in L/R^2 can be offset by adjusting the gas density and filling factor according to the rules of a class (2) transforma-

tion. For example, if we take the angular radius of NGC 1068 to be 2", then a reduction of N from 6×10^4 cm^{-3} to 1.5×10^4 cm^{-3} and an increase in f by a factor of two would lead to the same ionization structure and only small changes in the collisional suppression of the high excitation forbidden lines.

The crucial fact is that although the luminosities of NGC 1068 and NGC 7027 differ by a factor of a million, their surface brightnesses are very nearly the same. This implies that it is physically meaningful to apply a given ionization model to both objects.

(3) The effect of parameter changes

We now consider the effect of changes in the gas density, filling factor, and ionizing radiation in Model 1 in order to see what limits are placed on these parameters by the observed high excitation line intensities. Table 5 lists the parameters of the models.

(a) Gas density

We have seen that there must be large density fluctuations in NGC 1068, and in Model 1 these are described by a volume filling factor f. The observed radius and luminosity of the nebula require that the gas density and filling factor be related by $f \propto N^{-2}$. In order to study

TABLE 5

SUMMARY OF MODELS FOR NGC 1068

Model	Type of Ionizing Spectrum	2^+ ν_c T_b	Geometry*	N (cm^{-3})	R (pc)	Remarks
1	BB	175,000°K	F	$6x10^4$	120	Good fit to high excitation line intensities.
2	BB	175,000°K	F	$6x10^3$	120	[S III] too weak. This sets lower limit to r.m.s. gas density.
3	BB	175,000°K	F	$6x10^5$	120	[S III] too strong and [Ne III] too weak. This sets upper limit too r.m.s. gas density.
4	Exp.	7.5 Ryd	F	$6x10^4$	130	[O I] and [S III] too strong. This shows that artificial radial cutoff is necessary.
4a	Exp.	7.5 Ryd	F	$6x10^4$	70	Radial cutoff for correct I(λ6300). [S III] and [Ne III] too weak. This makes exponential spectrum unattractive.

TABLE 5 (CON'T)

SUMMARY OF MODELS FOR NGC 1068

Model	Type of Ionizing Spectrum	2^{+} T_b^c	Geometry*	N (cm^{-3})	R (pc)	Remarks
5	Power law	-0.85	F	$6x10^4$	280	Same as Model 4.
5a	Power law	-0.85	F	$6x10^4$	80	Same as Model 4a. Also a power law spectrum is ruled out by X-ray observations.

† T_b for black body spectrum, ν_c for exponential, or α for power law.

* F means a ball of filaments.

the effect of changing the gas density in Model 1, Models 2 and 3 were calculated with $N=6\times10^{3}$ cm^{-3}, f= 3.7×10^{-3} and $N=6\times10^{5}$ cm^{-3}, $f=3.7\times10^{-7}$, respectively.

The normalized line intensities of these models are given in Table 4. Of the high excitation lines, only [Ne V], He II, and [S III] change by more than about 30 percent between any of Models 1, 2, and 3. For $N<2\times10^{5}$ cm^{-3}, the recombination lines are quite insensitive because of the class (3) structural similarity determined by the ionizing photon frequency distribution. For $N=6\times10^{5}$ cm^{-3}, helium is not completely ionized in the outer part of the region where $\tau_{\nu}(4\ \text{Ryd})\lesssim1$, and hence the He I line intensities increase at the expense of the He II lines. Also, for $N=6\times10^{5}$ cm^{-3}, $I(\lambda5007)/I(H\beta)$ drops slightly because of collisional suppression and $I(\lambda3426)$ drops considerably because neon is not ionized up to Ne^{+4} except very close to the continuum source. The most sensitive high excitation line is [S III] λ9532. The reason is that the ionization potential of S^{+2} is less than 4 Ryd, and therefore sulphur is ionized above S^{+2} in the He^{+} zone if the density is low. The original choice of $N=6\times10^{4}$ cm^{-3} cm^{-3} was fortunate in giving the correct [S III] line intensity, and this supports the determination by Miller and Mathews (1972) from the [O III] and [N II] lines of NGC 7027. The [A III] lines,

not calculated in these models, are expected to behave similarly to [S III].

The conclusion is that although a wide range of gas densities is present in NGC 1068, most of the high excitation line radiation comes from filaments in which the r.m.s. gas density is close to 6×10^4 cm^{-3}.

(b) Ionizing radiation

We now consider the effect of changing the ionizing radiation energy distribution while keeping the total ionizing photon luminosity the same. A model similar to Model 1 but with T_b = 150,000° K gave I(λ4686) = 0.38 and I(λ3426) = 0.8, relative to I(Hβ), while T_b = 200,000° K gave I(λ4686) = 0.62 and I(λ3426) = 1.5 The rest of the high excitation lines showed little change, because the photon flux between 1 Ryd and 4 Ryd is much less sensitive to these changes in T_b than is the flux beyond 4 Ryd. The low excitation line intensities were not sensitive to these changes in T_b. The main result is that T_b = 175,000° K is favored by the [Ne V]/[Ne III] intensity ratio as well as by the He II to H I recombination line ratio.

Next we consider changes in the form of the ionizing radiation distribution. Table 6 gives the line intensities of Model 4, which differs from Model 1 in

TABLE 6

LINE INTENSITIES IN MODELS 4 and 5

Ion	λ	Model 4*	Model 4a	Model 5*	Model 5a
		$L_\nu \propto \exp(-\nu/7.5\nu_o)$		$L_\nu \propto \nu^{-0.85}$	
		R=130pc	R=70pc	R=280pc	R=80pc
[Ne V]	3426	1.2	N.C.	1.0	N.C.
He II	4686	0.56	N.C.	0.41	N.C.
[O III]	4363	0.30	N.C.	0.32	N.C.
[O III]	5007	23	N.C.	27	N.C.
[Ne III]	3869	0.6	0.4	1.4	0.5
[S III]	9532	1.2	0.6	4	0.5
H β	4861	1.0	N.C.	1.0	N.C.
He I	5876	0.13	0.12	0.15	0.14
[N II]	5755	0.017	0.010	0.020	0.009
[N II]	6583	1.1	0.5	1.4	0.3
[O II]	7325	0.10	0.08	0.12	0.09
[O II]	3727	0.08	0.03	0.17	0.025
[S II]	4072	0.004	0.001	0.026	$<10^{-3}$
[S II]	6720	0.018	0.004	0.26	$<10^{-3}$
[O I]	6300	2.9	0.4	8	0.4

*Radial cutoff at $Ne/N=10^{-2}$. [SII] is much stronger for a cutoff at $Ne/N=10^{-3}$.

†Radial cutoff to give correct I(λ6300). N.C. means no change for the smaller radius.

These models show that power law and exponential models are inferior to black body models because (1) they require artificial radial cutoffs and (2) because [Ne III] is too weak.

having $L_\nu = L_o \exp[-(\nu-\nu_o)/\nu_c]$, with $L_o = 2.1 \times 10^{27}$ ergs s^{-1} Hz^{-1} and $\nu_c = 7.5$ Ryd. If we let $h\nu_c = kT_s$, then $T_s = 1.2 \times 10^{6o}$ K; hence this continuum resembles the thermal bremsstrahlung from an optically thin plasma at 1.2×10^{6o} K. The outer boundary of the nebula was imposed at the point where $N_e/N = 10^{-2}$. Most of the high excitation lines are in good agreement with the observations; but a slight increase in the neon abundance would improve the fit, as was true for Model 1. The worst failure of Model 4 is that [S III] λ9532 and [O I] λ6300 are much too strong. This emission comes mostly from outside $R(H^+)$, where the ionization is due to penetrating X-rays. If there was no gas outside $R \simeq 1.4R(H^+) \simeq 70$ pc, then λ6300 would have the observed intensity. In this model (Model 4a), [S III] has only about half the observed intensity, but an increase in the sulphur abundance would improve the agreement. However, [Ne III] is weakened by the cutoff in R enough that $I(\lambda3869)/I(\lambda3426)$ is uncomfortably low. This occurs because the X-rays act on inner shell electrons to ionize neon beyond Ne^{+2} in the He^+ zone. In conclusion, an exponential continuum model probably could be doctored up to fit the high excitation line spectrum of NGC 1068; but Model 1, requiring no arbitrary radius cutoff, seems to be a

more natural explanation.

Model 5 is similar to Models 1 and 4, except that $L_\nu = L_o(\nu/\nu_o)^\alpha$, with $L_o = 4 \times 10^{27}$ ergs s^{-1} Hz^{-1} and $\alpha = -0.85$. The line intensities, given in Table 6, are similar to those of Model 4 in that the high excitation lines are in agreement with the observations except for [S III], which is much too strong. The high intensities of [O I] λ6300, [S II] λ6720, and [S III] λ9532 are the result of the relatively large amount of energy in penetrating X-rays in the power law continuum. Again, we must assume a radius cutoff, this time at $R \simeq 1.1R(H^+)$, to keep I(λ6300) from exceeding the observed value. As with Model 4a, this model (Model 5a) results in I(λ9532) and I(λ3869)/I(λ3426) having only about half the required values. Thus the power law and exponential continuum models have similar difficulties.

The ionizing continua assumed in Models 1, 4, and 5 are shown in Figure 1. The power law continuum has a flux in the 2-10 keV band that is two orders of magnitude greater than the observed upper limit (Kellogg 1972). The required radius cutoff implies that the radiation in this frequency band is not absorbed in the nucleus. It therefore appears that a power law ionizing continuum is ruled out for this object.

(c) Helium abundance

The observed intensity of He I λ5876 in NGC 1068 is slightly less than in NGC 7027. Thus one final parameter variation was to reduce the helium abundance to N(He)/N(H) = 0.08 in Model 5, in order to see whether this change had a large effect on the forbidden line intensities. The expected reduction of I(λ5876) was found, and there were small reductions in [O III] and [Ne III] while [Ne V] increased. These changes are due to the larger volume occupied by the He^{++} zone. The variation of [Ne III]/[Ne V] with helium abundance was discussed by MacAlpine (1972). The important point here is that the reduced helium abundance caused no changes large enough to upset the conclusions reached above.

(4) Conclusions

The conclusion of this section is that the high excitation line spectrum of NGC 1068 and NGC 7027 can be understood in terms of a simple model in which the line emitting gas is ionized and heated by an ultraviolet continuum. In the most successful model, the ionizing radiation source is a black-body with T_b = 175,000° K. The gas density is close to 6×10^4 cm^{-3} in the high excitation region. This gas occurs in con-

densations which occupy only 4×10^{-2} of the volume in NGC 7027 and 4×10^{-5} in NGC 1068. Thus extreme density fluctuations exist in NGC 1068. The mass of ionized gas in this model of NGC 1068 is about 10^5 $M_\odot$.

(D) The low excitation region

None of the preceeding models for the high excitation regions of NGC 1068 and NGC 7027 accounts for the low excitation lines of either object. In general, given the radius cutoffs required in Models 4a and 5a, the models all have the low excitations lines too weak. In Model 1, [O I] λ6300 and [S II] λ6720 are about right for NGC 7027; but the rest of the low excitation lines are too weak by factors of 3 to 10. In Model 4a, similar remarks apply except that [S II] λ6720 is also too weak because the radius cutoff, chosen to given the observed [O I] intensity, eliminates the S^+ region. It is clear that if either of these models represents the true nature of the high excitation region in either NGC 1068 or NGC 7027, then a different region is responsible for the low excitation lines. This conclusion is in harmony with the observational fact that the high excitation lines agree between NGC 1068 and NGC 7027, whereas the low excitation lines do not. In terms of the present models, the explanation is simply that the

high excitation regions are similar but radiate only weakly in the low excitation lines; the latter come from other regions which are different in the two objects. The purpose of this section is to investigate the nature of the low excitation regions.

(1) Observational comparison

As was remarked earlier, the low excitation lines are all stronger in NGC 1068 than in NGC 7027, with the exception of [O II] λ7325. The line ratios of [N II], [O II], and [S II] indicate some systematic difference between the physical conditions in the two objects. In Table 7 we compare the line ratios for these ions. These ratios are given as the intensity of the transition originating from the upper term divided by the intensity of the lower transition, and this ratio is smaller in NGC 1068 for each ion. This could be interpreted as a lower temperature or a lower density in NGC 1068. However, a temperature change alone seems unlikely because the difference required seems unreasonably large for [O II] and [S II], say from 12,000° K in NGC 7027 to 6,000° K in NGC 1068, and because the intensity ratio difference is smallest for [N II], which has the largest energy difference and thus the greatest temperature sensitivity. On the other hand, [N II] λ6583 is

TABLE 7

COMPARISON OF LOW EXCITATION LINE RATIOS
IN NGC 1068 AND NGC 7027

Ion	R (line ratio)	R(1068)	R(7027)	$\frac{R(1068)}{R(7027)}$
[O III]	$\frac{I(\lambda 7325)}{I(\lambda 3727)}$	0.12	0.92	0.13
[S II]	$\frac{I(\lambda 4072)}{I(\lambda 6720)}$	0.50	2.6	0.19
[N II]	$\frac{I(\lambda 5755)}{I(\lambda 6583)}$	0.021	0.048	0.44

collisionally suppressed by more than 50 percent for $N_e \lesssim 10^5$ cm^{-3}, whereas [O II] and [S II] are suppressed for $N_e \lesssim 10^4$ cm^{-3}. Thus a reduction from $N_e \approx 10^5$ cm^{-3} in NGC 7027 to $N_e \approx 10^4$ in NGC 1068 could account for the changes of all three line ratios. In reality, a range of densities is likely to exist; but an appropriate shift of the density distribution could lead to similar results.

(2) Low excitation emission near R(H^+)

We now investigate whether the low excitation line emission from the outer parts of Models 1 or 4 might be increased by adding a low density component in this region. Model 2, which has the low excitation lines much too weak, shows that this will not work in the black-body spectrum case. There is not enough ionizing radiation left in the narrow $H^+ \rightarrow H^0$ transition region. Furthermore, the emission from a component with N = 6×10^3 cm^{-3} added to Model 1 can only be reduced from that in Model 2 by the absorption of ionizing radiation by the main gas component at N = 6×10^4 cm^{-3}.

There is more hope for Model 4, in which the penetrating X-rays provide energy in the region outside R(H^+). If we assume the gas density is low enough in this region that hydrogen, and with it oxygen and nitrogen, are ionized, then the large amount of energy in [O I]

emission might be converted to [O II] and [N II]. At a density of 6×10^4 cm^{-3}, hydrogen is about one to ten percent ionized in the region just outside $R(H^+)$. Thus a reduction of the density to 10^3-10^4 cm^{-3} in this region would result in hydrogen being mostly ionized there. This could be accomplished by assuming that the density decreases abruptly beyond $R(H^+)$. Alternatively, we might assume that there is some low density gas in the space between the $N=6\times10^4$ cm^{-3} filaments throughout the nebula. Inside $R(H^+)$, where the ionization in the dense gas is relatively low, the emission of the dense gas is much higher than that of the low density gas. However, where the ionization in the dense gas is relatively low, the emission from the low density gas is relatively greater.

For example, consider a point beyond $R(H^+)$ where $N_e/N = 0.05$ in filaments with $N_1 = 6\times10^4$ cm^{-3} and filling factor f_1. In intermingled filaments with $N_2 = 6\times10^3$ cm^{-3} and filling factor f_2, the ionization is $N_e/N \approx 0.5$. The volume averaged forbidden line emission from the two regions is in the ratio $\bar{J}_2/\bar{J}_1 \approx 0.5N_2^2f_2/0.05N_1^2f_1 = 0.1f_2/f_1$. On the other hand, in the highly ionized region inside $R(H^+)$, we have $N_e/N \approx 1$, and thus $\bar{J}_2/\bar{J}_1 \approx 0.01f_2/f_1$. Hence for $f_2/f_1 \approx 30$, the gas at $N = 6\times10^4$ cm^{-3} dominates the high excitation emission, while

the lower density dominates the low excitation emission. More detailed calculations are now in progress to check this idea. Preliminary results for Model 4 indicate that it is difficult to get sufficiently strong [O II] emission by this scheme.

(3) Shadows of optically thick filaments

Another possible source of low excitation line emission is brought to mind by Van Blerkom and Arny's (1972) suggestion that strong [O II] emission may be expected from the shadows of optically thick globules in planetary nebulae. The word "shadow" in this context means the region away from the central star, where the gas receives only the diffuse nebular radiation, and not the starlight. Van Blerkom and Arny's calculation requires modification because it neglects helium. The helium recombination radiation in the shadow region raises the degree of ionization of some elements, and it increases the energy input per photoionization and hence increases the temperature. My rough calculations indicate that $T \simeq 13{,}000°$ K in the shadows in the He^+ zone, and that [O II] λ3727 is the strongest emission line for $N_e \simeq 10^4$ cm^{-3}.

The strength of the λ3727 emission from the shadow region supports the idea that the missing low excitation

line radiation in Model 1 might come from the shadows of many optically thick, dense filaments or globules in the high excitation region, because λ3727 is very weak in all the preceeding models. Davidson (1972) encountered a similar problem in his QSO models, and he postulated a large envelope at low density to get the required [O II] emission. The shadow idea may be an alternative in this case also.

Since He I Lyman radiation ionizes S^+, narrow, optically thin shadows do not provide a source of [S II] emission. However, in an optically thick shadow the helium secondary radiation may be absorbed before the hydrogen Lyman continuum. Van Blerkom and Arny's calculation would apply in the inner region, which could be a source of [S II] emission.

(4) Cloud collisions

Another possible source of low excitation emission is the ionization resulting from collisions of neutral gas clouds at speeds of order 100 km s^{-1}. The emission line widths in Seyfert galaxies indicate the presence of mass motions rapid enough to lead even to relatively high ionization. Thus the cloud collision model deserves study as a possible source not only of the low excitation emission but of the high excitation emission as

well (cf. Osterbrock 1971; Daltabuit and Cox 1972).

(E) Conclusions

A comparison of the reddening corrected emission line intensities of the Seyfert galaxy NGC 1068 and the planetary nebula NGC 7027 shows that the high excitation lines agree very closely while the low excitation lines do not. This suggests that there are separate high and low excitation regions in these objects. A successful model of the high excitation region of NGC 7027 was given, and it was shown that this model applies to NGC 1068 as well. Thus the similar high excitation line spectra of both objects can be understood in terms of a single model. The best fit to the observations was obtained for Model 1, which has filaments with $N=6\times10^{4}$ cm^{-3} ionized by radiation with a black body distribution at $T_b=175{,}000^{o}$ K. This conclusion is important because most previous discussion has concerned power law ionizing radiation and its possible synchrotron origin. No detailed calculations were presented for the excitation regions; but it was suggested that the low excitation lines might be radiated by low density gas between the filaments near the ionization boundary, from the shadows of optically thick condensations in the high excitation region, or by gas clouds ionized by collisions at speeds

of order 100 km s^{-1}.

IV. 3C 120

(A) Introduction

The purpose of this chapter is to deduce the physical properties of the emission line region in the nucleus of the high redshift (z=0.033) Seyfert galaxy 3C 120 and to determine whether the ionized gas has an unusually large helium abundance. Regarding the strong helium lines in the spectrum of 3C 120, two alternative interpretations are presented. The first is that models with ionizing continua similar to those in Chapter III for NGC 1068 can be applied to 3C 120 if the helium abundance has the unusually large value N(He)/N(H) = 0.22. The second interpretation is that the helium abundance in 3C 120 has a smaller value, but the gas is ionized by X-rays. After a review of the observations and some general geometrical inferences, specific models of the BLR and NLR will be presented, first for the models with the high helium abundance and then for the X-ray models.

(1) Observations

The optical spectrum of 3C 120 (Shields, Oke, and Sargent 1972) shows broad permitted emission lines of H, He, and possibly Fe II; narrow forbidden lines; and a smooth continuum with no evidence of stellar

TABLE 8

REDDENING CORRECTED EMISSION LINE INTENSITIES OF 3C 120*

Ion	λ (Å)	I(λ)
[S III]	9532	0.04:
[O II]	7325	0.01:
[S II]	6720	0.08
H α	6563	2.8
[O I]	6300	0.07:
He I	5876	0.26
[O III]	5007	1.00
H β	4861	1.00
He II	4686	0.5
[O III]	4363	0.04:
H γ	4340	0.47
[Ne III]	3869	0.3:
[O II]	3727	0.07:
[Ne V]	3426	0.5:

*Relative to Hβ. L(Hβ) = 3×10^{42} ergs s^{-1}.

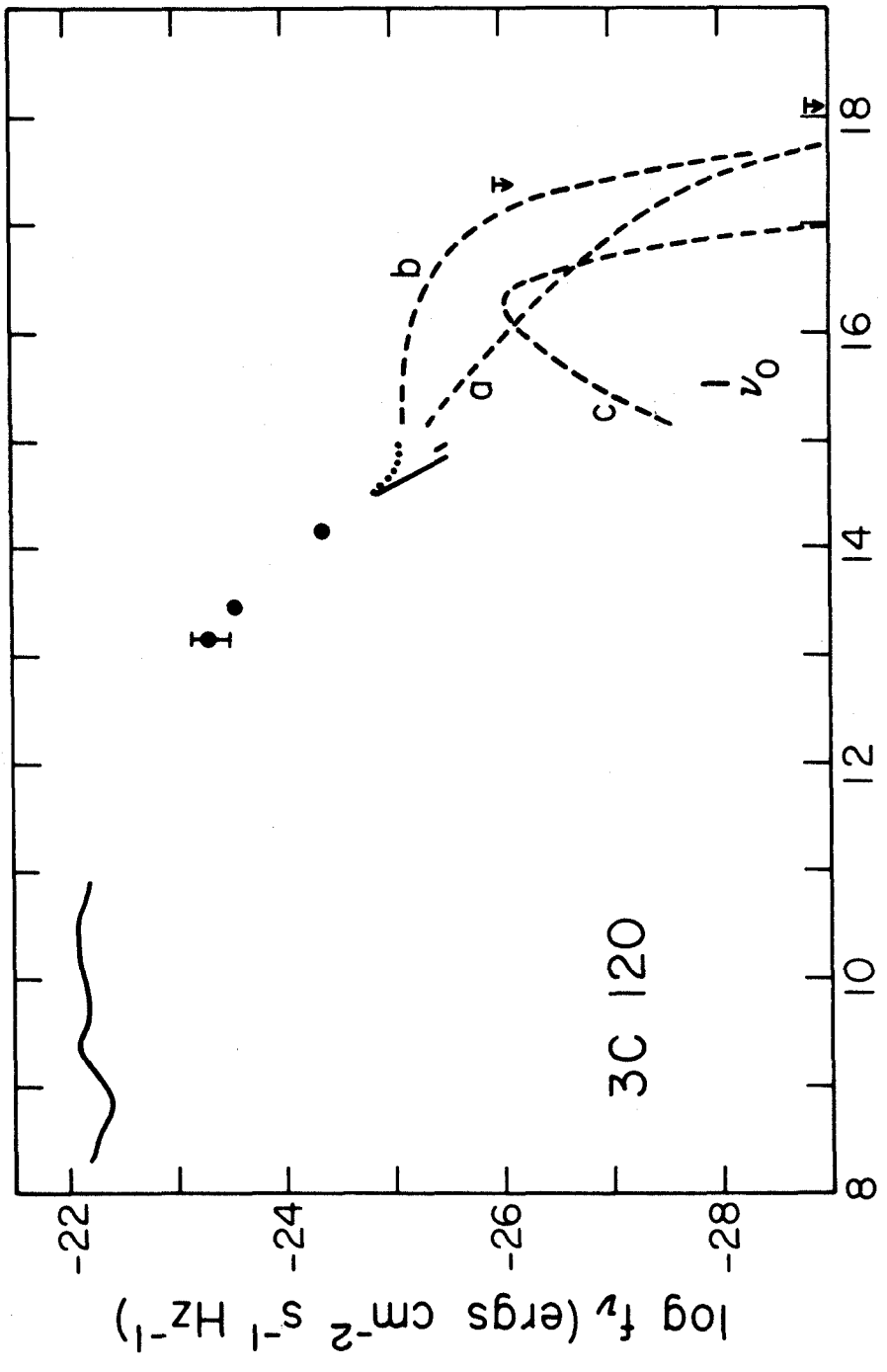

Fig. 5. - Observations of 3C 120 from Kellermann and Pauliny-Toth (1971), Rieke and Low (1972), Oke, Sargent, Neugebauer, and Becklin (1967), Shields, Oke, and Sargent (1972), Garmire and Riegler (1972), and Giacconi et al. (1972). The dotted curve represents the visual continuum corrected for reddening. The dashed curves show the ionizing continua in (a) Models 6 and 7; (b) Models 8, 9, 10, and 13; and (c) Model 11.

absorption features. The permitted lines have full half-widths of about 3000 km s^{-1}, while the forbidden lines have widths of about 200 km s^{-1}. Thus 3C 120 exemplifies the NGC 4151 type of Seyfert galaxy having a distinct broad line region and narrow line region. The line profiles show that the contribution of the NLR to the cores of the hydrogen and helium lines is less than about 20 precent; but since the broad permitted lines are very strong, the ratio of Balmer emission from the NLR to forbidden line emission from the NLR could be the same as in other Seyfert galaxies such as NGC 4151 or NGC 1068. The hydrogen and helium line decrements (Table 8) agree with the theoretical values for radiative recombination if a reddening correction corresponding to $A_V = 0^m.8$ and the Seaton (1960) reddening function are used. The reddening corrected continuum is flat in the UV and rises steeply in the near IR. The extrapolation of the flat near UV continuum to ionizing frequencies would easily provide enough ionizing photons to maintain the ionization of the line emitting gas. Figure 5 shows how the UV continua assumed in the following models compare to the optical and X-ray observations.

(2) Geometrical inferences

Shields, Oke, and Sargent (1972) showed that the mass and volume of the NLR far exceed those of the BLR, even though the BLR is considerably more luminous. An observational lower limit to the extent of the BLR is implied by the fact that the Hα and Hβ line fluxes remained constant to within about 2 percent over a period of two years while the continuum intensity decreased by about 20 percent. This suggests that the BLR is at least several light years across and is only sparsely filled by small, dense clouds or filaments of gas. This in turn implies that the broad line wings are caused by mass motions rather than by electron scattering, which requires a compact cloud of ionized gas.

It seems likely that the emission line region of 3C 120 does not completely surround the radiation source. One reason is that the observed near UV continuum is flat after correction for reddening, and its hypothetical extrapolation to higher frequencies would provide several times more radiation than required to ionize the emission line region. Another reason is that free-free absorption would prevent radio waves from traversing the emission line region. If it is assumed

that the compact radio source and the ionizing radiation source coincide, then the rapid radio variations (Shaffer et al. 1972) can be interpreted as meaning that we are seeing through a hole in the emission line region.

(B) Models with a large helium abundance

In this section, we show that if the ionizing radiation is similar to that in NGC 1068, then the helium abundance in 3C 120 is abnormally large. Comparing the normalized, reddening corrected helium line intensities of 3C 120 and NGC 1068, we see that I(λ4686) is about the same for the two objects, but I(λ5876) is about three times larger for 3C120. From equation II-25, we therefore find that N(He)/N(H) ≈ 0.24 in 3C 120. In the rest of this section, we shall adopt a large helium abundance of approximately this value.

In §IV-B-1, we present a model of the BLR and show that the density and radius of the BLR are restricted to a fairly narrow range of values. In §IV-B-3, we discuss models for the NLR of 3C 120. We estimate the size of and the range of densities in the NLR, and suggest what lines should be more accurately measured to provide a critical test of the models. The important

parameters of all the models in this chapter are listed in Table 9.

(1) The broad line region

Figure 6 gives the fractional abundances of some important ions in Model 6, which consists of a ball of small, optically thin filaments extending from R = 0 to a sufficiently large radius (1.5 pc) to absorb essentially all of the ionizing radiation from the point source in the center. The filaments have $N = 10^9$ cm^{-3}, volume filling factor $f = 10^{-6}$, the heavy element abundances in Table 3, and N(He)/N(H) = 0.22. The ionizing continuum has the form $L_\nu = L_o(\nu/\nu_o)^{-0.85} \exp(-\nu/\nu_c)$, with $L_o = 0.5 \times 10^{29}$ ergs s^{-1} Hz^{-1} and ν_c = 50 Ryd. The exponential cutoff was introduced to avoid conflict with the Uhuru upper limit to the X-ray flux from 3C 120 (Kellogg 1972). A model without this cutoff had nearly the same hydrogen and helium recombination line intensities, but slightly stronger Lyα.

The line intensities in Model 6 are given in Table 10. The recombination line intensities agree well with the observations of 3C 120, and they are relatively insensitive to the exact values of N and f as long as

TABLE 9

SUMMARY OF MODELS FOR 3C 120

Model	Type of Ionizing Spectrum	$\alpha^{\dagger}$ ν_c T_b	$\frac{N(He)}{N(H)}$	Geometry	N (cm^{-3})	R (pc)	Remarks
6	Power law	-0.85	0.22	F	10^9	1.5	Sets lower limit to density in BLR, and confirms abnormal helium abundance required for conventional ionization structure.
7	Power law	-0.85	0.22	F	2×10^6	50	Demonstrates presence of densities of at least 2×10^6 in the NLR.
8	Exp.	19 Ryd	0.12	S	1.5×10^{10}	3	Shows that X-ray ionization is an alternative explanation of strong He I lines.
9	Exp.	19 Ryd	0.12	S	3×10^{10}	0.3,30	Show effect of geometry in X-ray models.
10	Exp.	19 Ryd	0.12	F	3×10^{10}	40	

TABLE 9 (CON'T)

SUMMARY OF MODELS FOR 3C 120

Model	Type of Ionizing Spectrum	$\alpha^{\dagger}$ ν_c T_b	$\frac{N(He)}{N(H)}$	Geometry*	N (cm^{-3})	R (pc)	Remarks
11	BB	3×10^{5}°K	0.12	F	10^{11}	13	Show effect of form of ionizing spectrum in X-ray models.
12	BB	10^{6}°K	0.07	F	10^{11}	30	
13	Exp.	19Ryd	0.12	F	2×10^{6}	40	Shows that [Ne III] is too weak in X-ray models. Favors high helium abundance.

† T_b for black body, ν_c for exponential, α for power law.

*F for ball of filaments, S for thin shell.

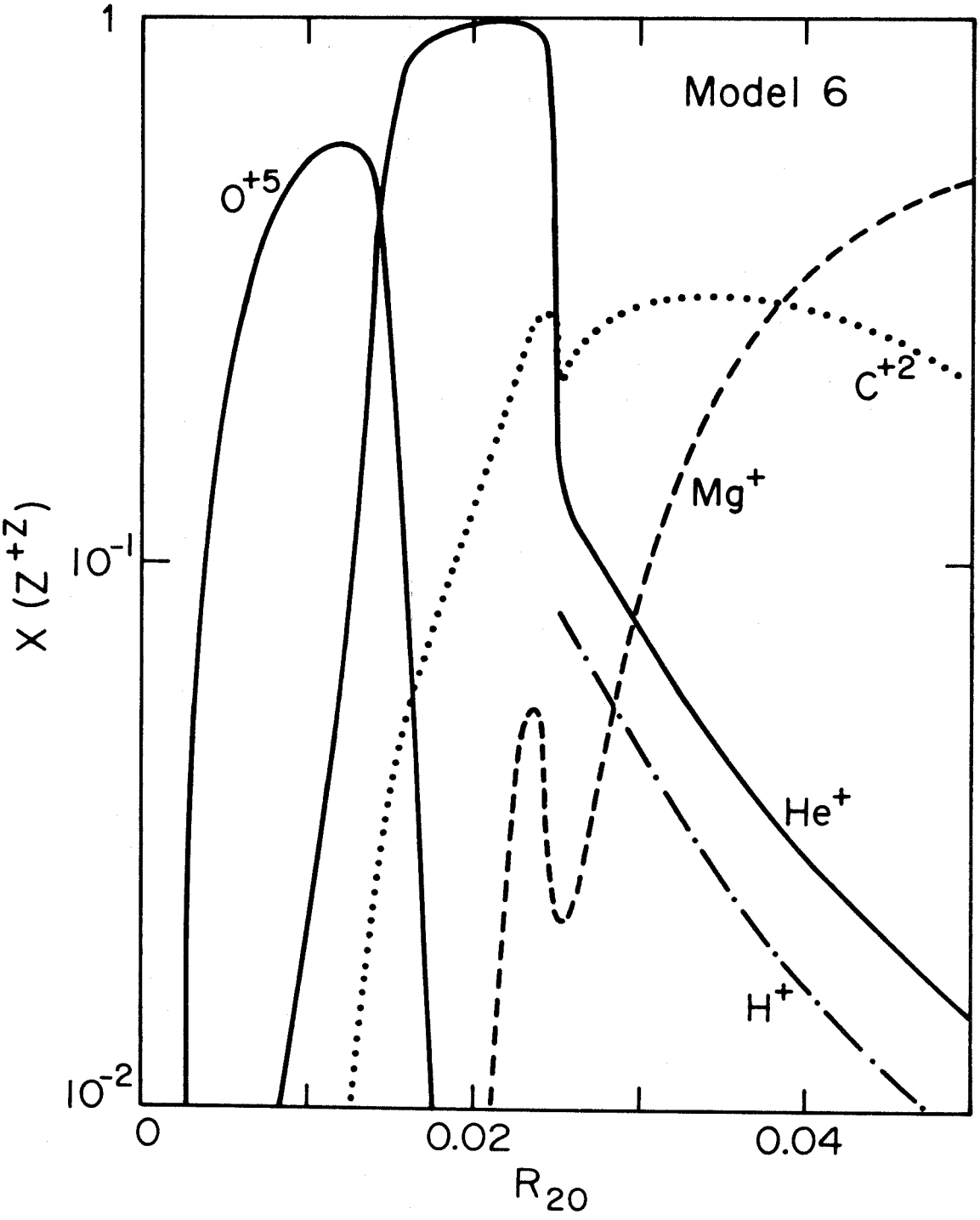

Fig. 6. - Ionization of hydrogen, helium, carbon, magnesium, and oxygen in Model 6.

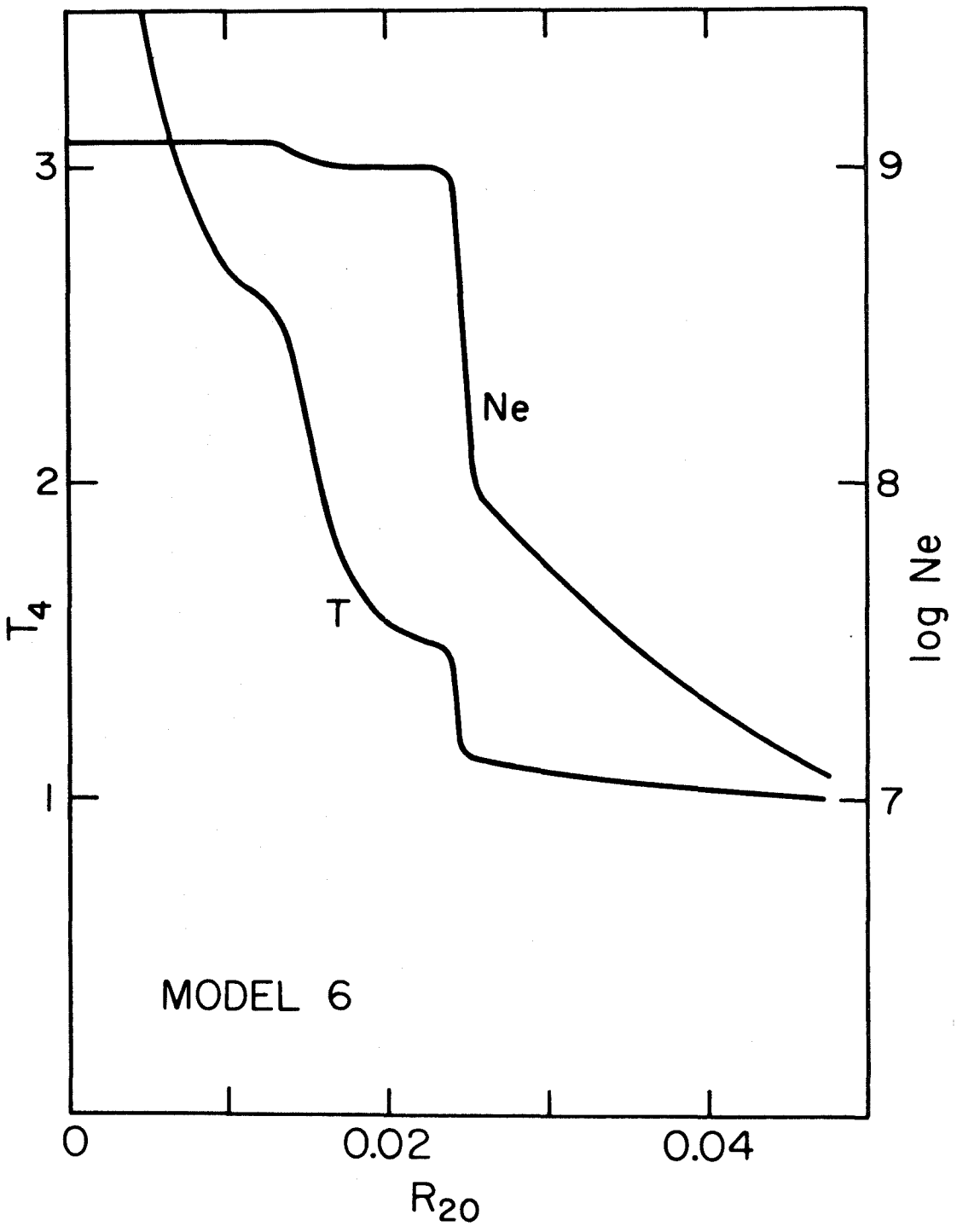

Fig. 7. - Electron density and temperature in Model 6.

TABLE 10

LINE INTENSITIES IN MODELS 6 AND 7.*

Ion	λ	Model 6 (BLR) $N=10^9 cm^{-3}$ R=1.5pc	Model 7 (NLR) $N=2x10^6 cm^{-3}$ R=50pc
H β	4861	1.00	1.00
Ly α	1216	42	40
He I	5876	0.25	0.26
He II	4686	0.45	0.45
C II]	2326	0.4	0.4
C III]	1909	4	7
C III]	977	0.5	0.8
C IV	1549	48	31
[N II]	6583	0.001	0.15
N IV]	1486	1.3	0.7
N V	1240	5	2.6
[O I]	6300	0.07	1.0
[O II]	3727	$<10^{-3}$	0.002
[O II]	7325	0.003	0.14
[O III]	5007	0.06	14
[O III]	4363	0.08	0.9
O VI	1035	15	3.4
[Ne III]	3869	0.06	1.1
[Ne V]	3426	0.02	0.8
Mg II	2798	2.3	0.9

TABLE 10 (CON'T)

LINE INTENSITIES IN MODELS 6 AND 7.*

Ion	λ	Model 6 (BLR) $N=10^9 cm^{-3}$ R=1.5pc	Model 7 (NLR) $N=2x10^6 cm^{-3}$ R=50pc
[S II]	6720	$<10^{-3}$	$<10^{-3}$
[S II]	4068	0.005	0.001
[S III]	9069	0.04	0.4

*$L_\nu \propto \nu^{-0.85}$ exp(-ν/50 Ryd). I(Lyα) includes a contribution of 25I(Hβ) from recombination. Model 6 shows that $N=10^9 cm^{-3}$ is the minimum density consistent with the absence of wings of λ4363 and λ3869, and that the abnormal helium abundance N(He)/N(H) = 0.22 is required.

the product Nf^2 is large enough that the gas is highly ionized. However, further models have shown that $N = 10^9$ cm^{-3} is the lowest density that will prevent the broad wings of [O III] λ4363 and [Ne III] λ3869 from exceeding the observational upper limits of about 1/20 the intensity of Hβ. For a density of 10^9 cm^{-3}, the radius of the He^{+2} zone must be no larger than about 1 pc. For a larger radius, the ionization of helium is not complete in this zone and λ4686 is too weak. This radius upper limit is close to the lower limit set by the lack of Balmer line intensity variations. If Model 6 is valid for 3C 120, this implies that the radius of the BLR is close to 1 pc and that the gas density is in the range 10^9-10^{10} cm^{-3}.

Alternative models with black-body or exponential ionizing continua can be constructed by transforming the models of NGC 1068 in Chapter III and correcting for the reduction in the volume of the He^{+2} zone due to the large helium abundance. The essential point is that I(λ4686)/I(Hβ) is nearly the same for both NGC 1068 and 3C 120. This implies that as far as the recombination lines are concerned, any ionizing spectrum which works for NGC 1068 will also work for 3C 120. The overabundance of helium in 3C 120 is inferred entirely on the

basis of the large intensity of the HeI lines. The same basic conclusions are reached in these cases as well, namely that R≈1 pc and that $N \approx 10^9$ cm^{-3}. Thus these values are well determined independently of the exact form of the ionizing radiation spectrum.

With the possible exception of the Fe II lines, which I have not analyzed, the permitted lines in the optical spectrum of 3C 120 provide little further information about the structure of the BLR. However, some of the ultraviolet resonance and intercombination (spin forbidden) lines are sensitive to the parameters of the model. Of particular interest are O VI λ1035 from the inner part of the nebula, and Lyα, C II], C III], and Mg II from the outer edge. Further information on the BLR will depend largely on satellite observations of these and other UV lines.

(2) The narrow line region

We now consider the region (NLR) which produces the relatively narrow forbidden lines in the spectrum of 3C 120. In order to set limits on the size and density of the NLR, we begin by considering a variety of models in which the chemical abundances and ionizing radiation are the same as in Model 6. Most of the con-

clusions will also apply to the case of black-body or exponential ionizing radiation. An exploratory series of models was calculated for hollow shells of gas with $R_i = 10^2$, 10^3, 10^4 pc. The density $N = 10^3$ cm^{-3} was chosen on the basis of the observed [O II] line ratio. The normalized line intensities of these models are given in Table 11. The choice $R_i = 10^2$ pc is ruled out because neon is too highly ionized in the He^{+2} zone to account for the observed strength of [Ne V] λ3426. This results from the large radiation flux L/R^2 at this small radius. On the other hand, $R_i = 10^4$ pc is ruled out because the ionization of neon is too low, and because the lines of [O I],[S II], and [S III] are much too strong relative to [O III] and [Ne III]. Thus the gas is restricted to the range $R \simeq 10^{2.5}$-$10^{3.5}$ pc, if $N = 10^3$ cm^{-3}.

With R in the required range, however, the theoretical intensities of the [O II] lines are too weak. Thus in the case of 3C 120, as in the case of NGC 1068, we are led to postulate separate low and high excitation line regions. The high excitation region contains densities much higher than the value indicated by the [O II] line ratio. For all the models in Table 11, the ratio I(λ5007)/I(λ4363) is much larger than observed.

TABLE 11

SERIES OF SHELL MODELS TO ESTABLISH THE SIZE OF THE NLR*

Ion	λ	R = 10^4 pc	10^3 pc	10^2 pc
Hβ	4861	1.00	1.00	1.00
He I	5876	0.36	0.26	0.25
He II	4686	0.11	0.49	0.52
C II]	2326	2	0.4	0.01
C III]	1909	0.2	4	0.05
C IV	1549	0.01	30	7
[N II]	6583	20†	0.7	0.01
[O I]	6300	15	2.9	0.06
[O II]	3727	2	0.7	0.007
[O II]	7325	0.10	0.04	0.001
[O III]	5007	7.4	36	27
[O III]	4363	0.015	0.41	0.21
[O VI]	1035	$<10^{-3}$	1.4	62
[Ne III]	3869	1.07	1.0	0.8
[Ne V]	3426	0.01	1.0	0.16
Mg II	2798	5	0.8	0.2
[S II]	6720	6	0.06	0.01
[S II]	4072	0.3	0.005	0.001
[S III]	9532	33	1.1	0.05

*$L_\nu \propto \nu^{-0.85} \exp(-\nu/50\ \text{Ryd})$, $N=10^3\ \text{cm}^{-3}$, $N(He)/N(H)=0.22$.
R_i is the inner radius of the thin gas shell; the radial cutoff was at $N_e/N=10^{-2}$. †Nitrogen charge exchange not used.

For $N < 10^6$ cm^{-3}, this ratio depends only on the electron temperature, which in turn depends rather weakly on the shape of the ionizing radiation spectrum and on the degree of ionization of the gas. For the above models with $N = 10^3$ cm^{-3}, and for a similar series of models with $N = 10^5$ cm^{-3}, it was found that the temperature was close to 13,000° K, given the deduced limits on R_1. This leads to the value $I(\lambda5007)/I(\lambda4363)=$ 100, whereas the observations indicate that this ratio is $\sim$25. The implication is that a large part of the [O III] radiation arises in gas with $N_e \gtrsim 2\times10^6$ cm^{-3}, where there is substantial collisional deactivation. Further support for this conclusion comes from the ratio $I(\lambda3869)/I(\lambda5007)$, which is too low for the 10^3 cm^{-3} and 10^5 cm^{-3} models, but is about right for the amount of collisional suppression of $\lambda5007$ indicated by the [O III] line ratio.

Thus we are led to a picture of the NLR of 3C 120 in which the low excitation lines come from a region with $N\sim10^3$ cm^{-3} and the high excitation lines come from a region containing densities in excess of 10^6 cm^{-3}. This is similar to the picture deduced for NGC 1068. Since a wide range of densities is present, one may expect that a completely successful model will have to take into

account a very complicated gas distribution. Nevertheless, we shall see what further progress can be made using a single density for the high excitation part of the forbidden line region.

From the results in Table 11, it is easy to calculate that for $N \simeq 10^{6.5}$ cm^{-3} in the high excitation region, a radius of $\sim$10-30 pc will come closest to providing enough [Ne V] emission. It is interesting that this is roughly the linear size indicated by the angular dimensions of the nearby Seyfert nuclei such as NGC 1068 and NGC 4151, although for 3C 120 the size was deduced from spectroscopic considerations alone. The volume filling factor of the filaments is very small ($\sim 10^{-6}$), although in reality the space may be at least partially filled with gas at a lower density.

These conclusions are illustrated by Model 7, which consists of a ball of filaments with $N = 2 \times 10^{6}$ cm^{-3} and $f = 2 \times 10^{-6}$. The ionizing radiation and chemical abundances are the same as in Model 6. The line intensities are given in Table 10, which shows that the high excitation line intensities are in fairly good agreement with the observations. The outer cutoff R = 50 pc was chosen to give the right intensity of [O I] λ6300, and this cutoff also leads to good agreement for [S III] λ9532.

As in the case of NGC 1068, the necessity of the cutoff favors ionization by black-body radiation.

The observed intensities of the [Ne III] and [Ne V] lines are somewhat uncertain, but they do suggest that [Ne V] is at least as strong as [Ne III]. The failure of Model 7 to yield enough [Ne V] emission could be improved by evacuating an inner cavity to eliminate the region where neon is ionized beyond Ne^{+4}; however, the shell models indicate that it is not easy to get [Ne V] as strong as [Ne III]. The reason is that the large helium abundance causes the He^{+2} zone to occupy a relatively small fraction of the total ionized volume. The sensitivity of the [Ne III]/[Ne V] intensity ratio to the helium abundance was emphasized by MacAlpine (1972). (Davidson [1972] has pointed out that the neglect of $O^{+5} \rightarrow O^{+4}$ dielectronic recombination may reduce the [Ne V] intensity. The reason is that the oxygen absorbs photons that would otherwise tend to increase the ionization of neon in the He^{+} zone. However, the shell models again suggest that this effect will not sufficiently increase the [Ne V] emission.)

Unfortunately, the present measurements of the neon line intensities are not accurate enough to provide a critical test. The measurement of λ3869 is made

difficult by blending with the broad He I λ3889 line, and it is possible that the measured [Ne V] intensities are affected by flourescent O III emission. In view of the significance of the [Ne III] and [Ne V] lines, as well as the [S III] lines which are sensitive to the value of NR^2/L, improved measurements of these lines would be especially useful.

(C) Models with X-ray ionization

We now show that X-ray ionization provides an alternative to a high helium abundance in 3C 120. Since the helium lines are observed only from BLR, we shall consider a variety of models for the BLR. Then we shall use the same ionizing continuum in models of the NLR. The physical basis for these models is that at frequencies above the helium ionization potential, the photoionization cross-section of He^0 is much greater than that of H^0. Therefore, in a region with NR^2/L so large that the gas is largely neutral, high frequency radiation ionizes helium to a greater degree than hydrogen. The resulting enhancement of the helium recombination lines can give the illusion of a large helium abundance.

(1) The broad line region

We begin with an example (Model 8) consisting of a thin shell or sheet of gas with $N = 1.5 \times 10^{10}$ cm^{-3} located 10^{19} cm $\simeq$ 3 pc from a point source of ionizing radiation with a spectrum given by $L_\nu = L_o \exp(-\nu/\nu_c)$, with ν_c = 19 Ryd. This continuum resembles the thermal bremmsstrahlung from an optically thin plasma at a temperature of 3×10^{6o} K. The value $L_o = 1.7 \times 10^{29}$ ergs s^{-1} Hz^{-1} was chosen to agree with the near UV observations (Figure 5). The helium abundance N(He)/N(H) = 0.12 used in this model is the smallest value that gives the He line intensities of 3C 120 correctly in models with an exponential ionizing continuum. If the continuum is extended to higher frequencies in an effort to achieve greater helium line enhancement, the resulting high energy photoelectrons cause enough collisional ionization of hydrogen to reduce the intensities of the helium lines relative to Hβ.

The ionization structure of the thin shell of gas in Model 8 is shown in Figure 8, which is a graph of the fractional abundances of several ions as a function of the distance outward from the inner edge of the shell. The main points are that nowhere are there abundant

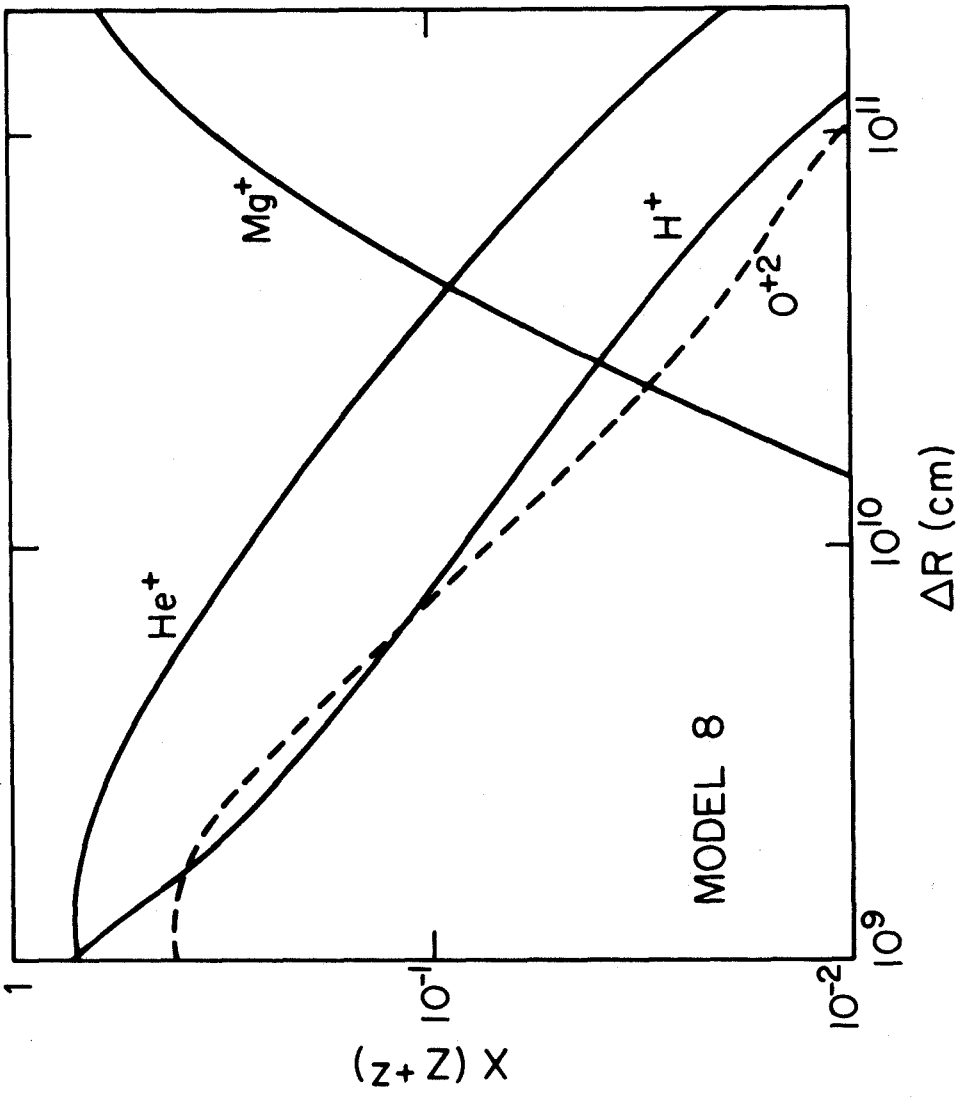

Fig. 8. - Ionization of hydrogen, helium, oxygen, and magnesium in Model 8.

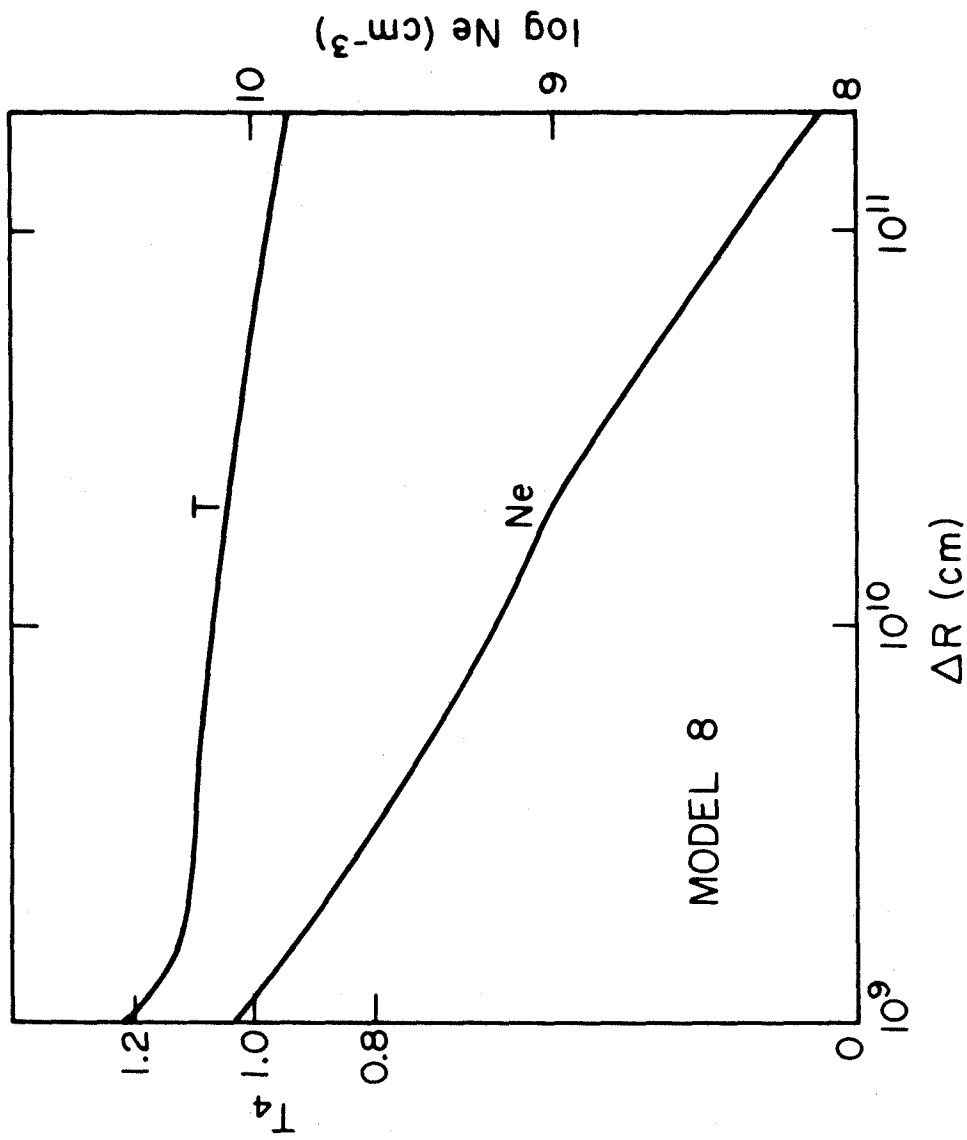

Fig. 9. - Electron density and temperature in Model 8.

ionization stages above about Z^{+3}, that H^0 is a major constituent throughout the nebula, and that there are no sharp ionization boundaries.

The relative line intensities in Model 8 are given in Table 12. The hydrogen and helium recombination line intensities agree with the observations in the visual frequency range; therefore to further evaluate this model we must consider the UV line intensities. These are useful for predicting what lines would be most interesting to observe when UV satellites of sufficient sensitivity become available, and they can also be compared with the UV line intensities of QSO's with sufficiently large redshifts. Compared to a typical QSO spectrum, the important features of Model 8 are the very strong collisionally excited lines of the abundant neutral or singly ionized species, expecially Lyα, C II], and Mg II. The reason is that the large energy input per photon requires that much more energy be radiated in collisional emission than in recombination emission; and relatively low ionization is needed for strong He I line enhancement. (If NR^2/L is small enough that the gas is highly ionized, then equation II-25 applies and there is no illusion of a large helium abundance.)

TABLE 12

EFFECT OF GEOMETRY ON LINE INTENSITIES IN X-RAY MODELS.*

Ion	λ	Model 8 (single sheet)	Model 9 (two sheets)	Model 10 (filaments)
H β	4861	1.00	1.00	1.00
Ly α	1216	240	135	160
He I	5876	0.27	0.24	0.27
He II	4686	0.41	0.45	0.46
He II	1640	2.8	3.1	3.1
C II]	2326†	6	8	8
C III	1909	5.0	1.0	3.0
C IV	1549	4.2	38	12
[O III]	5007	0.006	0.001	0.001
O VI	1035	0.002	12	0.56
Mg II	2798†	10	38	30

* $L_\nu \propto \exp(-\nu/20\text{Ryd})$

† Sensitive to radial cutoff, here taken at $Ne/N=10^{-3}$.

Most of the cooling in Model 8 is due to collisional excitation of hydrogen. This fact allows us to write a simple analytical estimate of T. Let $\langle h\nu-1 \rangle$ denote the mean kinetic energy of the photoelectrons in Ryd. Since $h\nu(Ly\alpha) = 3/4$ Ryd, thermal equilibrium requires that, on the average, a photoelectron causes $4/3 < h\nu-1>$ collisional excitations of hydrogen before recombining. From the mean collisional excitation cross-section $Q(1\rightarrow2) = 3.5 \times 10^{-17}$ cm^2 adopted by Goldsmith and Silk (1972), we find $d_{12}(H^0) = 2.6 \times 10^{-8} N_e T_4^{-1/2} 10^{-5.1/T_4}$ s^{-1}. With this expression and the equation of ionization equilibrium for hydrogen and helium, the thermal equilibrium equation is easily solved to give

$$T \approx \frac{10{,}400^\circ \text{ K}}{1 + 0.20 \log_{10}[\langle h\nu-1 \rangle^{-1} N(H^0)/N_e]} . \qquad \text{IV-1}$$

For the conditions in Model 8, the expression in brackets is close to unity, and hence T is near $10{,}500^\circ$ K as shown in Figure 9.

The limits on the density and radius in Model 8 are not as narrow as in Model 6, because Model 8 has a lower degree of ionization than is admissible in Model 6. The observational limits on the intensity of the [O III] and [Ne III] line wings show that N must

be greater than 10^9 cm^{-3} in models similar to Model 8; and this minimum density requires a radius R = 10 pc. For R = 1/3 pc, the observational lower limit, the required density is $N = 10^{12}$ cm^{-3}. Thus the observations leave an uncertainty of a factor of 30 in R and 10^3 in N, for the adopted value of L_o, which is an upper limit.

(a) X-ray models with different geometry

The geometrical arrangement of the gas in the BLR of 3C120 probably has a complex distribution in density and radius. We now consider models which have the same ionizing radiation and chemical abundances as Model 8, but which have a more complex geometry.

Model 9 consists of optically thick filaments or sheets of gas with a density of 3×10^{10} cm^{-3}. Some of the filaments are 10^{20} cm from the ionizing radiation source (these filaments will be called the low ionization zone = LIZ), and the rest of the filaments are at $R = 10^{18}$ cm (high ionization zone = HIZ). The important parameter in distinguishing the LIZ from the HIZ is NR^2. In the HIZ, helium is mostly He^{+2}, and this region is the source of most of the He II line emission. On the other hand, helium is mostly He^0 in the LIZ, which

produces most of the He I line emission. The HIZ contributes 58 percent of the Hβ radiation in Model 9, and the LIZ contributes 42 percent. These contributions are proportional to the relative fractions of the ionizing radiation intercepted by the two types of filaments. The relative contributions of the HIZ and the LIZ can always be forced to give I(λ5876)/I(λ4686) correctly by adjusting the solid angle around the radiation source which the two types of filaments occupy. However, I(λ5876)/I(Hβ) then will be correct only if the ionizing radiation spectrum and the helium abundance are properly chosen. It was found that for a given helium abundance, the strongest He lines occurred for ν_c = 20 Ryd, and this value of ν_c requires N(He)/N(H) = 0.12 to fit the spectrum of 3C 120. This result is the same as found for Model 8.

The line intensities in Model 9 are given in Table 12. Lyα is weaker relative to Hβ than in Model 8, and Mg II λ2798 is considerably stronger. This difference is due to the lower ionization in the LIZ of Model 9 than in Model 8. This leads to a greater abundance of Mg^+ and a lower electron temperature, which together cause more energy to come out as λ2798 at the expense of Lyα. The intensities of C IV λ1549 and especially O VI λ1035

are much greater than in Model 8, because C^{+3} and O^{+5} are abundant in the HIZ.

Model 10 has the same chemical abundances, gas density, and ionizing radiation as Model 9; but in Model 10, the filaments are optically thin and are uniformly distributed with volume filling factor $f = 3 \times 10^{-10}$ throughout a ball of radius $R_{max} = 1.4 \times 10^{20}$ cm. The density and filling factor are related so that the transition from the He^{++} zone to the He^{+} zone occurs at the right place to give the correct value of I(λ4686)/ I(λ5876). Table 12 lists the line intensities in Model 10. Compared to Model 8, Model 10 has weaker Lyα, and stronger Mg II, C IV, and O VI.

Comparison of Models 8, 9, and 10 shows which lines are most sensitive to the details of the gas distribution. The intensity of Lyα is not very sensitive, because it is determined mainly by the total power in the ionizing continuum. C II] varies by less than a factor of two because C^{+} is always abundant in the low ionization region providing the He I line enhancement. C IV and Mg II are strong in all three models but are more sensitive to the conditions. The strength of O VI λ1035 is extremely sensitive to the existence or absence of a region of high ionization. These properties help to define the most critical UV observations to test the X-ray models.

(b) X-ray models with different ionizing continua

We next turn to a considertion of the effect of changing the ionizing radiation spectrum. Models 11 and 12 illustrate the case of ionizing radiation is described by the Planck function (Equation III-1). In considering these models, one should bear in mind that for a given T_b, there is a minimum value of L_o to provide enough ionizing photons to account for L(Hβ). Larger values of L_o may be used if it is assumed that the gas does not completely surround the radiation source, as is probably the case. The homologies described earlier can be used to relate models of this type. The values of L_o chosen here are such that the black body radiation is a small part of the continuum of λ3500, but provides most of the radiation at ionizing frequencies.

Model 11 has $T_b = 3 \times 10^{50}$ K and $L_o = 1.7 \times 10^{29}$ ergs s^{-1} Hz^{-1}; the gas has the form of a ball of tiny filaments with $N=10^{11}$ atoms cm^{-3} and $f=4 \times 10^{-11}$. The line intensities are given in Table 13. The main differences between Models 10 and 11 are that the latter has somewhat weaker C II], C III], and Mg II. This is because the exponential cutoff of the black-body radiation in Model 11 occurs at a lower frequency, so there is less energy in penetrating X-rays in the peripheral region of

TABLE 13

EFFECT OF ENERGY DISTRIBUTION ON LINE INTENSITIES IN X-RAY MODELS.*

Ion	λ	Model 11 ($T_b=3\times10^{5}$°K)	Model 12 ($T_b=10^{6}$°K)
H β	4861	1.00	1.00
Ly α	1216	160	550
He I	5876	0.23	0.27
He II	4686	0.59	0.46
C II]	2326†	2.1(2.6)	6(14)
C III]	1909	0.9	6
C IV	1549	7	10
O VI	1035	0.22	0.4
Mg II†	2798	3(6)	7(70)

*Ionizing radiation has Planck distribution.

†Radial cutoff at $N/N=10^{-2}$. Values in parentheses are for $N/N=10^{-3}$.

low ionization.

Model 12 is another filamentary model with $N=10^{11}$ cm^{-3}, $f=10^{-10}$, $T_b=10^{60}$ K, and $L_o=1.7\times10^{29}$ ergs s^{-1} Hz^{-1}. The chemical abundances are the same as in the preceeding models except that N(He)/N(H)=0.07. The line intensities are given in Table 13. The relative hydrogen and helium line intensities in this model are close to those observed for 3C 120 in spite of a helium abundance only one-third as large as in the power law continuum Model 6. The collisional lines of the low ions, especially Lyα and Mg II, are much stronger in Model 12 than in the preceeding models because of the large number of energetic photons.

(c) Resonance scattering in the BLR

The intensities of the UV resonance lines may be reduced by the combined effects of resonance scattering and dust within the emission line region. O'Dell (1965) has shown that in a nebula with a large optical dept τ_α in the center of the Lyα line, the distance traveled by a typical Lyα photon before escape is about 10 times the radius of the nebula. Unfortunately, the calculation of τ_α in models of Seyfert galaxies is uncertain because we do not know the velocity gradients in the emission line region. For the X-ray models discussed

here, $\tau_\alpha \approx 10^7$ for thermal Doppler broadening, but $\tau_\alpha \approx 10^4$-10^5 if there are small scale velocity gradients corresponding to the observed line widths of $\sim 10^3$-10^4 km s^{-1}. In either case, τ_α is large. Therefore, if the extinction within the BLR of 3C 120 is more than a few hundredths of a magnitude, Lyα will be mostly absorbed by dust before it escapes. This is also true for the other optically thick resonance lines, such as C IV λ1549 and Mg II λ2798.

It is also possible that a significant fraction of the Lyα radiation in these models may be converted to the two-photon continuum. For the high electron density in the BLR, the probability of conversion per scattering of a Lyα photon is 1.3×10^{-8}, and the mean number of scatterings before escape is $\sim 10\tau_\alpha$ (O'Dell 1965). The values of τ_α estimated in the last paragraph indicate that conversion may be likely if the BLR consists of large clouds with relatively small internal velocities.

(d) Collisional excitation of the Balmer lines.

The strong collisional Lyα emission in the X-ray models suggests that there may be a large collisional contribution to the Balmer lines as well. Using the rate coefficients given by MacAlpine (1971), we easily

find

$$\frac{I^C(H\alpha)}{I^C(Ly\alpha)} = \frac{E_{23}q(1\rightarrow 3)}{E_{12}q(1\rightarrow 2)} = 0.11\ T_4^{-1/3}\ \exp(-2.2/T_4). \qquad \text{IV-2}$$

Since T_4 is close to unity in the X-ray models, $I^C(H\alpha)/I^C(Ly\alpha) \approx 0.012$. For Models 9, 10, and 11, $I^C(Ly\alpha) \approx 100$, and therefore $I^C(H\alpha) \approx 1$. If this Hα emission is added to the Hα recombination emission, $I^R(H\alpha) = 2.8I^R(H\beta)$, the total is $I(H\alpha) = 4I^R(H\beta)$. The collisional contribution to Hβ is probably small, but accurate excitation coefficients to n=4 and higher would be useful to check this. Shields, Oke, and Sargent (1972) found I(Hα) = 4.0, but they attributed this large value to interstellar reddening because the other hydrogen and helium lines indicated the same amount of reddening. If the reddening explanation is correct, then the X-ray models probably can be ruled out on the basis of the predicted collisional emission in Hα. On the other hand, if there is very little reddening of 3C 120, then the Hα intensities in Models 9, 10 and 11 agree well with the observations; but Model 12 and probably Model 8 still are ruled out. More accurate observations of the Paschen and He I lines would be useful to settle this issue.

(e) Summary of X-ray Models for the BLR

These models predict very strong collisionally excited lines of the low ionization stages of H, C, and Mg. Although there is considerable variation in the line intensities of different models, we can identify some basic differences between the "conventional" spectrum models and the normal helium abundance models with X-ray ionization. Table 14 compares a composite observed QSO spectrum (Davidson 1972) with the high helium abundance Model 6 and with a representative average of Models 8 through 12. This comparison shows that UV line observations, especially of Lyα, C II], and Mg II would determine whether any of the preceeding X-ray models describes the actual situation in the nucleus of 3C 120.

(2) The NLR

We now consider some models for the NLR of 3C 120 which use the same ionizing radiation spectrum as Models 8, 9, and 10, namely $L_\nu = 1.7 \times 10^{29}\ e^{-\nu/\nu c}$ ergs s^{-1} Hz^{-1}, with ν_c = 19 Ryd. The purpose of these models is to determine whether there are any key forbidden line intensities which may serve to confirm or disprove the X-ray ionization picture. An exploratory series of

TABLE 14

COMPARISON OF CONVENTIONAL AND X-RAY MODELS FOR THE BLR

Ion	λ	Model 6	X-ray*	QSO†
H β	4861	1.00	1.00	1.00
Ly α	1216	42	$\geq$150	40.0
He I	5876	0.25	0.26	----
He II	4686	0.45	0.5	$\leq$0.3
He II	1640	3.2	3.5	$\leq$3
C II]	2326	0.4	8	----
C III]	1909	4	4	2
C IV	1549	48	10	9
[O III]	5007	0.06	0.00	2
O VI	1035	15	0-10	----
Mg II	2798	2.3	5-50	1.5

*Representative values from Models 8-12

†Composite spectrum from Davidson (1972).

shell models was computed for the same chemical abundances as Model 8 with N = 10^3 and 10^5 cm^{-3}, respectively. The relative line intensities were similar to those in Table 11 for the power law models. Thus the basic geometrical conclusions found for the power law models also hold for the exponential continuum models. Specifically, distinct low excitation and high excitation regions must be postulated. In the high excitation region, a density of $\sim 10^6$ cm^{-3} is required for the correct [O III] line ratio. Such a density implies a radius of 10-30 pc and a small volume filling factor.

It is interesting that these conclusions do not depend on the form of the ionizing radiation spectrum. Most important, it might be thought that X-ray ionization could lead to a high enough temperature to explain the [O III] line ratio without a high gas density. These calculations show that this is not the case. Hence the high temperature in the NLR proposed by Shields, Oke, and Sargent (1972) is rejected.

In order to look for critical differences between the X-ray and high helium abundance models for the NLR, a filamentary model similar to Model 7 was computed with N = 2×10^6 cm^{-3}, f = 6×10^{-7}, N(He)/N(H) = 0.12, and the above exponential ionizing spectrum. A cutoff at R = 40 pc

was chosen to give the observed intensity of λ6300. In contrast to Model 7, this model (Model 13) had $I(\lambda 3869)/I(\lambda 3426) \simeq 0.1$, much smaller than observed. The reason is that the volume of the He^{+2} zone is relatively larger because Model 13 has a greater fraction of photons with $\nu > 4$ Ryd and because the helium abundance is smaller. Furthermore, X-rays acting on the inner shell electron ionize Ne^{+2} in the He^{+} zone. This is similar to the effect found in Chapter III from a comparison of the black body models with the exponential and power law models. Therefore, it is difficult to get [Ne III] strong enough in the X-ray models, and this is evidence against X-ray ionization and for an abnormally large helium abundance in 3C 120. Further calculations are under way to determine whether 3×10^{5o} K black body radiation (Model 11) and an appropriate nebular geometry can result in stronger [Ne III] emission. It would also be useful to have a more accurate measurement of [Ne III].

(D) Conclusions

Several conclusions about the geometry of the emission line regions depend very little on the nature of the ionizing radiation. The BLR is smaller, more dense, and much less massive than the NLR. The BLR has $N > 10^9$ cm^{-3}, $M < 100 M_\odot$, $R \sim 1$ pc; and it probably consists of

narrow filaments about 1 a.u. thick. The density lower limit found here is an order of magnitude higher than previously assumed, and this is important because it leads to rather definite conclusions about the size of the BLR. The NLR contains about 10^6 $M_\odot$ of gas in the form of filaments with $N \sim 2 \times 10^6$ cm^{-3} spread over a region about 30 pc in radius. A much larger mass of gas at a lower density may be present in the space between or outside these filaments. The low excitation emission requires another source, and densities of the order of 10^3 cm^{-3} are involved. Thus the NLR of 3C120 closely resembles the whole emission line region of NGC 1068, and the great difference between the spectra of the two objects is due mainly to the addition of a very small mass of rapidly moving gas near the center of 3C 120.

The existing data indicate that 3C 120 has an unusually large helium abundance, N(He)/N(H) = 0.22, and that the ionizing radiation spectrum resembles that of a black body near 175,000° K. Thus 3C 120 has an energy source similar to that of NGC 1068 although more luminous, but the helium abundance in 3C 120 is roughly three times as large as that in NGC 1068. Ionization by X-rays could explain the strong helium emission lines of 3C 120 without an abnormal helium abundance, but other line intensities seem to be in disagreement with this model.

However, in view of the importance of the helium abundance issue, the X-ray explanation should be checked by improved optical observations, by measurement of certain critical UV lines, by more sensitive X-ray observations in the 1 keV range, and by infrared observations that might provide evidence of the huge amounts of energy involved in the X-ray models.

V. CONCLUSIONS

The most important result of this investigation is that the most likely source of ionization in Seyfert galaxies is ultraviolet radiation with an energy distribution similar to black-body radiation at a temperature of $1.5\text{-}2\times10^{5}$° K. The radius of a black body providing the minimum ionizing photon luminosity at 175,000° K is 2×10^{13} cm ≈ 1 a.u. for 3C 120 and one-third of this for NGC 1068. This conclusion is in contrast to the power law ionizing continua which have been emphasized in previous models of QSO's and Seyfert galaxies. However, it is noted that Kaneko (1972) suggested ionization by black-body radiation for NGC 1068 on the basis of (1) the similarity of the spectrum to that of NGC 7027 and (2) the positive spectral index resulting when the visual nonstellar continuum adopted by Visvanathan and Oke (1968) is corrected for the reddening displayed by the emission lines.

The choice of black-body radiation is preferred over the alternatives of power law or exponential continua because (1) the latter required artificial radial cutoffs in the gas distribution whereas the black-body model does not, (2) the power law and exponential models predict [Ne III] to be weaker than is observed, and (3) the power law spectrum is ruled out for NGC 1068 by X-ray observa-

tions. The essential feature distinguishing the black body spectrum is that the flux falls off rapidly with frequency in either direction from the peak. By concentrating the ionizing photons near a few Ryd frequency, we can have a large enough fraction of photons with $\nu>4$ Ryd to account for the He II line intensities without having a large X-ray flux. Other peaked energy distributions with steep high frequency cutoffs could have the same advantages as the black body spectrum.

Another important conclusion is that in spite of great differences between the spectra of NGC 1068 and 3C 120, these objects are very similar in regard to ionization mechanism and nebular geometry. Most of the mass and volume in each object are due to a region of gaseous filaments with densities ranging from $\sim 10^6$ cm^{-3} down to $\sim 10^3$ cm^{-3}, filling only a small fraction of a region about 50 pc in radius. The high excitation line spectra can be understood in terms of photoionization by an ultraviolet continuum with the same spectrum in both objects. The low excitation spectra have a different origin which also appears to be the same in both objects. These conclusions follow primarily from the simple fact that within the observational uncertainty margins, the relative forbidden line intensities in NGC 1068 and 3C 120 are the same. The similarity of the

ionizing radiation is further demonstrated by the fact that I(λ4686)/I(Hβ) is the same in both objects, even though the permitted line radiation in 3C 120 comes from a different region than the forbidden line emission. The significant exception to the agreement of the forbidden line intensities is that there is more collisional suppression of [O III] in 3C 120. This implies that the gas density distribution extends to slightly higher values in the NLR of 3C 120 than in NGC 1068, but this has no major effect on the geometrical picture.

The outstanding difference between the spectra of NGC 1068 and 3C 120 is the great strength of the broad permitted lines in the spectrum of 3C 120. These wings, which are the defining characteristic of the NGC 4151 type spectrum, arise from a separate broad line region of dense, rapidly moving gas as proposed by Souffrin (1968). The results here represent a considerable refinement of the picture presented by Shields, Oke and Sargent (1972) for 3C 120 because the ionization structure models lead to an increased lower limit to the density in the BLR and a well defined geometrical description of its relationship to the NLR. Specifically, we now know that the BLR occupies a region about 0.5-3 pc in radius, much smaller than the NLR. This fact is important to the explanation of the origin of the

high densities and velocities in the BLR. For example, the well defined distance of the BLR from the radiation source should facilitate the evaluation of the importance of radiation pressure.

The most important point regarding the geometrical picture is that the differences between the NGC 1068 and NGC 4151 type spectra are due to the presence of only 10^2 $M_\odot$ or less of rapidly moving gas near the center of a much more massive (10^5-10^6 $M_\odot$) emission line region which is very nearly the same in both types of Seyfert galaxy.

It is interesting to note that the volume averaged gas density in the objects studied is only about one atom per cm^3. This suggests that the gas involved may have been an ordinary interstellar medium before it was ionized and compressed into filaments at the beginning of the outburst in the nucleus. The high helium abundance in 3C 120 may be useful in criticizing this picture. As an example, let us consider the possibility that radiation pressure due to the ionizing continuum amplifies density fluctations in the nuclear interstellar medium and causes the gas to move outward. At first, the condensations near the center may be pushed to very high velocities and densities by the strong radiation flux close to the continuum source, thereby

forming the BLR of an NGC 4151 type Seyfert galaxy. As time passes, these dense filaments may be dispersed or driven out of the nucleus, while the less dense gas in the NLR acquires higher velocities. At this stage, the object may assume the appearance of NGC 1068, which has little or no BLR but has wider lines than those from the NLR of 3C 120.

This investigation suggests a number of observations that are especially important to improve our understanding of Seyfert galaxies. In the visual and ultraviolet frequency range, a few of the observations specifically related to the present models include the following:

(1) UV observations of the broad Lyα, C II], and Mg II emission from 3C 120 could decide whether the X-ray ionization hypothesis is correct, and thereby determine the helium abundance in the BLR.

(2) For both NGC 1068 and 3C 120, the black body ionizing radiation suggested by this study could lead to a rapidly rising flux near the Lyman limit considerably stronger than might be expected from extrapolation of the visual continuum.

(3) The high density and small thickness of the filaments forming the BLR of 3C 120 suggests that

that these filaments may be short lived (cf. Davidson [1972]), and therefore the Lyman continuum absorption may vary on a time scale as short as months or years.

(4) According to these models, the BLR of 3C 120 is not more than a few pc across, and therefore the intensities of the broad permitted lines may change on a time scale of about ten years.

(5) The strongest forbidden line emission from the BLR is likely to be [O III] λ4363 and [Ne III] λ3869, and this broad emission may be detectable with high resolution scanners. Such a detection would determine the density and radius of the BLR independently of the time variation argument.

(6) The most important visual observation relating to the NLR is the measurement of the intensity of [O III] λ4363, since this line indicates the presence of high densities in the NLR. Unfortunately, the measurement of λ4363 is made difficult by blending with Hγ. One approach would be to use a high resolution scanner to determine accurate profiles of the other Balmer lines and then to use this information to separate Hγ from λ4363. This measurement

might also show whether the gas with $N \gtrsim 10^6$ cm^{-3} is moving more rapidly than the lower density gas, as might be expected by analogy to the rapid motion of the very dense gas in the BLR.

X-ray observations of NGC 1068 have ruled out a power law ionizing continuum for this object, and observations of 3C 120 show that if the ionizing radiation has a power law distribution, then it must have a cutoff at energies of about 0.5 keV or less. A reduction of the upper limit in the 2-10 keV band by one or two orders of magnitude would rule out a power law continuum. A reduction of the 1 keV upper limit by an order of magnitude would rule out the exponential continuum in Model 6. Strong X-ray absorption would be interesting not only because of the implications regarding the connection between the X-ray and radio sources, but also because of the radial cutoffs required in some models.

Strong infrared emission from dust is a necessary consequence of the observed reddening of the nuclei of Seyfert galaxies. In the case of 3C 120, the infrared luminosity must be at least 10^{44} ergs s^{-1} in any model, and might be as high as 10^{46} to 10^{47} ergs s^{-1} if the X-ray models are correct. The lower limit of 10^{44} ergs s^{-1} follows simply from the known

visual extinction of almost 1^m and the knowledge that corresponding to the observed $L(H\beta) = 3 \times 10^{42}$ ergs s^{-1} there is at least 25 times as much energy in Lyα alone. If the dust lies near the outer edge of the NLR, around 100 pc from the continuum source, then it may be expected to radiate most strongly in the 10 micron region. This is important because the existing observations near 10 microns (Riecke and Low 1972) already rule out the X-ray models if the dust is this close to the nucleus. It is important to look for large infrared fluxes at longer wavelengths.

Finally, accoring to this investigation, the BLR of 3C 120 is within a few pc of the radiation source. It therefore would be interesting to look for evidence of an interaction between the gas and the radio source if a rapidly expanding radio component (Shaffer et al. 1972) can be followed for several years.

In closing, we turn to the relation of the Seyfert galaxies to the QSO's. The homology relations show that the spectra of these objects may not show any systematic dependence on luminosity if the radii of the nebulae increase as $L^{1/2}$. This homology is especially relevant to the issue of the distance of the QSO's. Any filamentary model can be scaled to smaller luminosity and distance, subject to the constraint that f is less than

unity. Since the filling factors discussed for QSO's are typically 10^{-4} (cf. MacAlpine 1972), and since the filling factor is inversely proportional to the distance in this transformation, we see that such a model can be scaled to as close as $10^{-4}D$, where D is the cosmological distance. Thus the line spectra alone will not provide an astrophysical parallax for QSO's. However, for QSO's much closer than the cosmological distance, the nebular radius (proportional to distance) would be so small that rapid variations of the line intensities would be expected.

APPENDIX

The usefulness of a detailed ionization structure program was discussed briefly in the Introduction. The main point is that the number of physical processes involved in photoionized nebulae is so large that computer calculations are required to make full use of the accurate photoelectric intensity measurements now available. The advantage is greatest where the exact value of the electron temperature is important, as in the argument for high densities in the NLR of 3C 120 based on the [O III] line ratio. The program is also useful for showing which line intensities are most sensitive to the model parameters, and which are too strong or too weak for any member of a certain class of models. Once the critical lines are recognized, a hand calculation may aid one's understanding of the problem; but the computer calculations can save a great deal of effort by drawing attention to the interesting lines.

The program used for this work calculated the equilibrium ionization and temperature in a spherically symmetric model nebula photoionized by a central point source of continuum radiation of black-body or power-law-times-exponential form. The gas could occupy a thin shell (essentially plane-parallel), a thick shell, or a ball, and could be either uniform or filamentary. Filamentary

models assumed infinitesimally thin filaments occupying a small fraction of the total volume, with empty space in between. There was provision for a low density interfilamentary medium, for intermingled filaments of a different density, and for densities and filling factors varying with radius; but little use of these features was made in the work discussed here because of the overwhelming number of possible arrangements. The outer boundary of the nebula usually was determined by the program at the point where N_e/N dropped to some specified small value.

The heavy element abundances (Table 3), taken from MacAlpine (1972), are supposed to represent values commonly found in the Galaxy. The present models show that the adopted oxygen and neon abundances are close to the actual values in NGC 1068 and with lower observational accuracy in 3C 120. Unfortunately, the abundances of the remaining heavy elements are not well determined. The abundance of helium was considered an unknown to be determined by the models.

The models were calculated by an iterative procedure to find self-consistent solutions of the fundamental equations discussed in §II-A. Beginning at the center or inner edge of the gas cloud, the program calculated

the ionization, temperature, opacity, optical depths, and line emission in a series of shells whose thickness was a small fraction (typically one or two percent) of the size of the ionized zone estimated from equation (II-21). The photoelectric ionization and heating rates per ion of each species were numerically evaluated according to equations (II-1) and (II-7), including all filled electron shells. The numerical integration typically used about 50 frequency intervals in which a_ν, τ_ν, and L_ν were assumed to vary as powers of the frequency. The contributions to the rates in each interval were obtained by interpolation between analytic solutions for the cases of small and large optical depths. Given these rates and an assumed electron temperature and density, the ionic abundances were calculated from equations (II-4) and (II-6). A new estimate of N_e was then found from equation (II-5), and the procedure was iterated to find a consistent solution for the ionization and electron density. The heating and cooling rates were then compared; and if they differed, then new values of the temperature were tried until the equilibrium value was found, with the ionization recalculated for each temperature. The emission in the lines and Balmer continuum was then found by multiplying the emissivity by the volume of the shell. The calculation then proceeded to the next shell, with an

increase in the optical depths as given by equation (II-17). In addition to the ionization, temperature, and optical depths, the emission line luminosities were recorded as a function of radius to show the dependence of the line intensities on the outer boundary. A considerable saving of computing time was achieved by neglecting the contribution to the heating and cooling by ions of elements other than hydrogen and helium whose fractional abundances were less than 10^{-3}, and by terminating the ionization rate integrations when the last frequency interval contributed less than two percent to the heating rate. The errors introduced by these omissions were tested for a variety of models and found to be negligible.

The valence shell photoionization cross-sections, collision strengths, and transition probabilities mostly were taken from the sources cited by MacAlpine (1972). For helium, the cross-section was taken from Brown (1971). The inner shell photoionization cross-sections were computed from the Stobbe formulae (Bearden 1966). Radiative recombination coffficients were taken from Seaton (1959) and Tarter (1971a,b).

The choice of the fundamental processes included and the numerical precision required involves considerations

such as the programming time, the cost of running the program, the accuracy of the atomic data available, and the kind of conclusions that are sought. The program used in this study involves several simplifications compared to those used by Davidson (1972) and MacAlpine (1972). One difference is that dielectronic recombination was neglected here. MacAlpine (1971) has compared the dielectronic and radiative recombination coefficients of a number of ions. The temperatures involved this the present work are too low for dielectronic recombination to be of major importance. The process is important for C^{+3} at 20,000° K. However, the only detailed consideration of the carbon lines here was in the X-ray models for 3C 120, where the temperature was only 10,000° K and dielectronic recombination was negligible.

The present models used the on-the-spot treatment of the ionizing diffuse radiation of hydrogen and helium. Hummer (1968) has reviewed the subject of radiative transfer in planetary nebulae. MacAlpine (1972) used OS for the line radiation and an outward-going transfer approximation for the Lyman continuum. Davidson (1972) considered transfer of both the line and continuum diffuse radiation. The justification of OS for the line radiation is that resonance scattering is likely to increase the path of helium Lyα photons enough that they are absorbed by

hydrogen before they move far from the point of origin. The OS approximation is not as good for the Lyman continuum, but the resulting error in the line intensities is not large because the volumes of the major ionization zones are determined by photon conservation (equations [II-21] and [II-22]), which is given correctly by OS. The intensities of the lines in the $H^+ \rightarrow H^0$ transition region are probably the most sensitive to transfer effects, and it would be useful to have calculations to study the differences resulting from various treatments of radiative transfer. However, the real geometry of Seyfert nuclei is complicated, and any treatment of transfer will be incorrect in detail. Therefore the usefulness of comparing various transfer approximations is mainly to estimate the accuracy beyond which no model calculation should be trusted. I have calculated some of the models by MacAlpine (1972) and Davidson (1972), and the differences resulting from radiative transfer, as well as atomic data, etc., were not large enough to seriously affect the conclusions reached here.

The present calculations assumed constant density, whereas Davidson (1972) used constant pressure. My calculations of Davidson's models using constant density show that the differences are not important. Furthermore, the density variation in an isobaric model is insignificant

compared to the huge range of densities present in Seyfert nuclei, and presumably there are comparable pressure fluctuations. Therefore, I feel that a constant pressure calculation holds little advantage over a constant density calculation. What is really needed is a physical theory of the dynamical state of the gas.

The validity of the conclusions reached depends on the accuracy of the atomic data used in the models. Photoionization cross-sections and recombination coefficients are particularly important for the ions whose lines are critical indicators of the physical conditions. One result of this investigation is that ionization of filled electron shells by the X-rays in exponential and power law continua can be important in testing the validity of these models. Accurate cross-sections for the inner shells of Ne^{+2} and S^{+2}, as well as their neighbor ions, would be especially useful in this regard. Another important physical effect is charge transfer. The validity of oxygen-hydrogen charge transfer should be investigated under a wide range of conditions, since this effect is partly responsible for the weakness of [O II] in the models, and the resulting conflict with the observations. The importance of (N^{+},H^{0}), (C^{+2},He^{0}), and (S^{+2},He^{0}) charge transfer should also be studied.

An especially important process neglected in most

ionization structure models is the absorption of ionizing radiation by internal dust. Heavy reddening of the emission lines of Seyfert galaxies is now established, and the extinction could be greater than assumed if there is dust mixed with the ionized gas (Mathis 1970; Münch and Persson 1971). Models with internal dust should be given high priority, at least to the extent of seeing what major changes in the line intensities can result.

REFERENCES

Aller, L., Bowen, I., and Wilson, O. 1963, Ap. J., 138, 1013.

Bearden, A. 1966, J. Appl. Phys., 37, 1681.

Brocklehurst, M. 1971, M.N.R.A.S., 153, 471.

_____. 1972, ibid., 157, 211.

Bahcall, J., and Kozlovsky, B. 1969a, Ap. J., 155, 1077.

_____. 1969b, ibid., 158, 529.

Brown, R. 1971, Ap. J., 164, 387.

_____. 1972, Ap. and Space Sci., 16, 274.

Brown, R., and Mathews, W. 1970, Ap. J., 160, 939.

Cox, D., and Tucker, W. 1969, Ap. J., 157, 1157.

Daltabuit, E., and Cox, D. 1972, Ap. J. (Letters), 173, L13.

Davidson, K. 1972, Ap. J., 171, 213.

Eilek, J., Auman, J., Ulrych, T., Walker, G., and Kuhi, L. 1972, Bull. A.A.S., 4, 231.

Garmire, G., and Riegler, G. 1972, Ast. and Ap. (in press).

Giacconi, R., et al. 1972 (in preparation).
Goldsmith, D., and Silk, J. 1972, Ap. J., 172, 563.
Hummer, D. 1968, I.A.U. Symposium No. 34, Planetary Nebulae, p. 166.

Hummer, D., and Mihalas, D. 1970, M.N.R.A.S., 147, 339.

Kaneko, N. 1972, Pub. Astr. Soc. Japan, 24, 145.

Karzas, W., and Latter, R. 1961, Ap. J. Suppl., 6, 167.

Kellermann, K., and Pauliny-Toth, I. 1971, Astrophys. Letters, 8, 153.

Kellogg, E. 1972, I.A.U. Symposium No. 55.

MacAlpine, g. 1971, Ph. D. Thesis (University of Wisconsin).

_____. 1972, Ap. J., 175, 11.

Mathis, J. 1970, Ap. J., 159, 263.
Miller, J. 1968, Ap. J. (Letters), 154, L57.
Miller, J., and Mathews, W. 1972, Ap. J., 172, 593.

Münch, G., and Persson, S. 1971, Ap. J., 165, 241.

O'Dell, C. 1962, Ap. J., 135, 371.

_____. 1963, ibid., 138, 1018.

_____. 1965, ibid., 142, 1093.

Oke, J. B. 1969, Pub. A.S.P., 81, 11.

Oke, J. B., Sargent, W., Neugebauer, G., and Becklin, E. 1967, Ap. J. (Letters), 150, L173.

Oke, J. B., and Schild, R. 1969, Ap. J., 161, 1015.

Osterbrock, D. 1962, Ap. J., 135, 195.

_____. 1971, Pontificiae Academiae Scientiarum, Scripta Varia, No. 35, p. 151.

Perek, L., and Kohoutek, L. 1967, Catalogue of Galactic Planetary Nebulae (Prague: Academia Publishing House).

Rieke, G., and Low, F. 1972, Ap. J. (Letters), 176, L95.

Rees, M., and Sargent, W. 1972, Comments Ap. and Space Sci., 4, 7.

Sandage, A. 1961, The Hubble Atlas of Galaxies (Carnegie

Institution of Washington).

Searle, L., and Sargent, W. 1968, Ap. J., 153, 1003.

Seaton, M. 1959, M.N.R.A.S., 119, 81.

Seaton, M. 1960, Rept. Progr. Phys., 23, 313.

Seyfert, C. 1943, Ap. J., 97, 28.

Shaffer, D., Cohen, M., Jauncey, D., and Kellermann, K. 1972, Ap. J. (Letters), 173, L147.

Shields, G., Oke, J. B., and Sargent, W. 1972, Ap. J., 176, 75.

Shields, G., and Oke, J. B. 1972 (in preparation).

Souffrin, S. 1968, Ann. d'Ap., 31, 569.

_____. 1969, Ast. and Ap., 1, 414.

Steigman, G., Werner, M., and Geldon, F. 1971, Ap. J., 168, 373.

Tarter, C. 1971a, Ap. J., 168, 313.

_____. 1971b, private communication.

Van Blerkom, D., and Arny, T. 1972, M.N.R.A.S., 156, 91.

Visvanathan, N., and Oke, J. B., 1968, Ap. J. (Letters), 152, L165.

Walker, M. 1968, A. J., 73, 854.

Wampler, E. J. 1971, Ap. J., 164, 1.

Weedman, D. 1972, Ap. J., 171, 5.

Williams, R. 1967, Ap. J., 147, 556.

_____. 1971, Ap. J. (Letters), 167, L27.

Williams, R., and Weymann, R. 1968, A. J., 73, 895.